(12)

Change No. 5

for

THE TRAPPED RADIATION HANDBOOK
(DNA 2524H)

21 January 1977

Instructions

The recipient is requested to remove the pages listed below from DNA 2524H, add the attached pages per DNA letter of approval dated 13 June 1977, and record this action on page iii.

Remove	Add
Title Page (4 January 1977)	Title Page (21 January 1977)
ii (4 January 1977)	ii (21 January 1977)
ix through x (4 January 1977)	ix through x (21 January 1977)
xv through xvi (2 December 1974)	xv through xviii (21 January 1977)
xvii through xviii (4 January 1977)	xxxv through xxxvi (21 January 1977)
xxxv through xxxvi (4 January 1977)	xxxix through xl (21 January 1977)
xxxix through xl (4 January 1977)	2-1 through 2-76 (21 January 1977)
2-1 through 2-6 (Original)	15-1 through 15-16 (21 January 1977)
2-7 through 2-8 (2 January 1973)	
2-9 through 2-10 (Original)	
2-11 through 2-12 (2 January 1973)	
2-13 through 2-32 (Original)	
2-33 through 2-34 (2 January 1973)	
2-35 through 2-66 (Original)	
15-1 through 15-18 (2 December 1974)	

Note: If the recipient did not receive a copy of DNA 2524H (The Trapped Radiation Handbook) plus changes 1 through 4, they can be obtained by addressing a request to the below named individual. A limited supply is available for this purpose.

M.J. Dudash
General Electric Company—TEMPO
DASIAC
816 State Street
Santa Barbara, CA 93102

(18) DNA 2524H-Change 5 (19)

(9) THE TRAPPED RADIATION HANDBOOK

Change 5

Compilers and Editors-in Chief:

(10) John B. Cladis
Gerald T. Davidson
Lester L. Newkirk

(11) Revised
21 January 1977

(12) 1977p.

Project Officer: Dr. Charles A. Blank

Prepared for:

Defense Nuclear Agency
Washington, D.C. 20305
by Lockheed Palo Alto Research Laboratory
(15) ~~Under Contract~~ DNA 001-73-C-0065
NWER ~~Subtask~~ HC047-08

Published by:

DASIAC
General Electric Company—TEMPO
Santa Barbara, California 93102
Under Contract DNA 001-75-C-0023
NWED Subtask DC008-01

21011

12

LIST OF EFFECTIVE PAGES

PAGE	LAST CHANGE	PAGE	LAST CHANGE
Title Page	21 January 1977	7-1 through 7-30	Original
ii	21 January 1977	8-1 through 8-2	1 November 1973
iii through iv	2 December 1974	8-3 through 8-4	Original
v through viii	1 November 1973	8-5 through 8-6	1 November 1973
ix through x	21 January 1977	8-7 through 8-8	Original
xi through xii	4 January 1977	8-9 through 8-10	2 December 1974
xiii through xiv	2 December 1974	8-11 through 8-12	Original
xv through xviii	21 January 1977	8-13 through 8-35	1 November 1973
xix through xxxiv	4 January 1977	8-35A through 8-35D	1 November 1973
xxxv through xxxvi	21 January 1977	8-36	1 November 1973
xxxvii through xxxviii	4 January 1977	8-37 through 8-80	Original
xxxix through xl	21 January 1977	8-81 through 8-82	2 January 1973
1-1 through 1-22	Original	8-83 through 8-84	Original
2-1 through 2-76	21 January 1977	8-85 through 8-86	1 November 1973
3-1 through 3-6	Original	8-87 through 8-88	Original
3-7 through 3-8	2 January 1973	8-89 through 8-90	1 November 1973
3-9 through 3-18	Original	9-1 through 9-36	Original
3-19 through 3-24	2 December 1974	10-1 through 10-9	Original
3-25 through 3-36	Original	11-1 through 11-34	Original
3-37 through 3-46	2 December 1974	11-35 through 11-36	2 January 1973
3-47 through 3-68	Original	11-37 through 11-60	Original
3-69 through 3-100	2 December 1974	12-1 through 12-6	Original
4-1 through 4-100	4 January 1977	13-1 through 13-20	Original
5-1 through 5-2	2 December 1974	14-1 through 14-2	Original
5-3 through 5-8	Original	14-3 through 14-4	2 January 1973
5-9 through 5-126	2 December 1974	**15-1 through 15-16**	21 January 1977
6-1 through 6-60	Original	**D-1 through D-10**	**4 January 1977**

CONTENTS

ILLUSTRATIONS

TABLES

AUTHORS

Section 1. John B. Cladis, Lockheed Palo Alto Research Laboratory.

Section 2. Lester L. Newkirk, Lockheed Palo Alto Research Laboratory; J.C. Cain, U.S. Geological Survey (Denver); W.P. Olson, McDonnell Douglas Astronautics Co.

Section 3. Gerald T. Davidson, Lockheed Palo Alto Research Laboratory.

Section 4. K.W. Chan, D.M. Sawyer, and J.I. Vette, NASA–Goddard Space Flight Center.

Section 5. Gerald T. Davidson, Lockheed Palo Alto Research Laboratory.

Section 6. Martin Walt, Lockheed Palo Alto Research Laboratory.

Section 7. Gerald T. Davidson, Lockheed Palo Alto Research Laboratory and Roy W. Hendrick, Jr., General Electric–TEMPO.

Section 8. David L. Crowther, William H. Harless, Jr., and J.W. Schallau, Lockheed Palo Alto Research Laboratory.

Section 9. A.M. Peterson and J.F. Vesecky, Stanford Research Institute.

Section 10. John B. Cladis and Billy M. McCormac, Lockheed Palo Alto Research Laboratory.

Section 11. "Supplementary Topics:"

- Section 11.1. George H. Nakano, Lockheed Palo Alto Research Laboratory.
- Section 11.2. Charles H. Humphrey, Lockheed Palo Alto Research Laboratory.
- Section 11.3. Albert D. Anderson, Lockheed Palo Alto Research Laboratory.

Section 11.4. Fred H. Saga, III, General Electric—TEMPO.

Section 11.5. Lester L. Newkirk, Lockheed Palo Alto Research Laboratory.

Section 12. John B. Cladis, Lockheed Palo Alto Research Laboratory.

21 January 1977

SECTION 2

THE GEOMAGNETIC FIELD

L.L. Newkirk, Lockheed Palo Alto Research Laboratory
J.C. Cain, U.S. Geological Survey (Denver)
W.P. Olson, McDonnell Douglas Astronautics Co.

2.1 INTRODUCTION

The geomagnetic field is generated by various sources located within the Earth and the surrounding ionosphere and magnetosphere. The internal sources include the core field produced by electric currents flowing near the core surface (2,900-kilometer depth). This source dominates all others below five Earth radii, exerting the controlling force for particle trapping. The main field near the Earth can be represented to an accuracy of about 90 percent by a tilted dipole at the Earth's center. The remaining 10 percent consists of a spectrum of higher order terms of decreasing importance, down to sizes of about 4,000 kilometers. Features having sizes smaller than this are thought to be mainly caused by direct magnetization of crustal material. Although the very local anomalies, observed even at aircraft altitudes, are sometimes sufficiently intense to double or reverse the field, their effect has decreased to a small fraction of the total field by ionospheric heights.

The effects of magnetospheric and ionospheric currents are relatively small below a few Earth radii. At low satellite altitudes (e.g., 500 kilometers), about a fraction of a percent from orbit-to-orbit can be observed, even during relatively quiet conditions, because of the variations of these external sources and the response of the conducting Earth to their changes (see subsections 2.5 and 2.6).

The core field exhibits a slow "secular" variation that is characteristically a fraction of a percent change in intensity per year. This phenomenon is regional; that is, its scale is not dominated by the dipolar component. The dipolar component is weakening about 5 percent per century.

In some studies involving trapped radiation, and particularly beyond 5 R_E, the (tilted) dipole approximation of the field is adequate. In many studies, however, a more accurate representation is required: a spherical harmonic expansion of a scalar potential fitted

to measured values of the field. Beyond 6 R_E, currents produced by charged particles in the magnetosphere and at the boundary of the magnetosphere begin to become comparable to, and eventually dominate, the ambient field configuration.

Numerical models of the geomagnetic field are thus most accurate at low satellite altitudes where the main contribution is from the Earth's core, and become less certain at greater distances because of the variability of the external effects. Very precise estimates, even at low altitude, must include these external sources for any but extremely quiet conditions.

The geomagnetic field, like other large-scale phenomena found in nature, is never absolutely quiescent or undisturbed. Field measurements versus time show a variety of disturbances having time durations lasting from a fraction of a second to as long as several days. The patterns are irregular in some cases and smooth in others, and might have a partially periodic or oscillatory structure. The amplitude variations range from a small fraction of one nanotesla (1 nT = 1 γ = 10^{-5} gauss) to several hundred nT. Many of the disturbances are localized events, but others encompass a significant portion of the magnetosphere. Some of the disturbances undoubtedly play a strong role in the particle supply and loss processes that determine the intensities of radiation belts.

The numerous types of magnetic disturbances, along with their causes, are discussed in subsequent portions of this section. Appendix 2A describes some of the magnetic indices used in trapped radiation studies to characterize the relative intensities of magnetic disturbances.

2.2 MAGNETIC FIELD ELEMENTS

The historical representation of the elements of the geomagnetic field are shown in Figure 2-1. The total field vector is denoted in the literature by either $\overline{B}$ or $\overline{F}$ (the Russians prefer $\overline{T}$). $\overline{B}$ is used here. The elements X, Y, and Z are north, east, and vertically down in a geodetic system. As shown in Figure 2-2, there are slight rotations from the geocentric components normally given by B_θ, B_φ, and B_r.

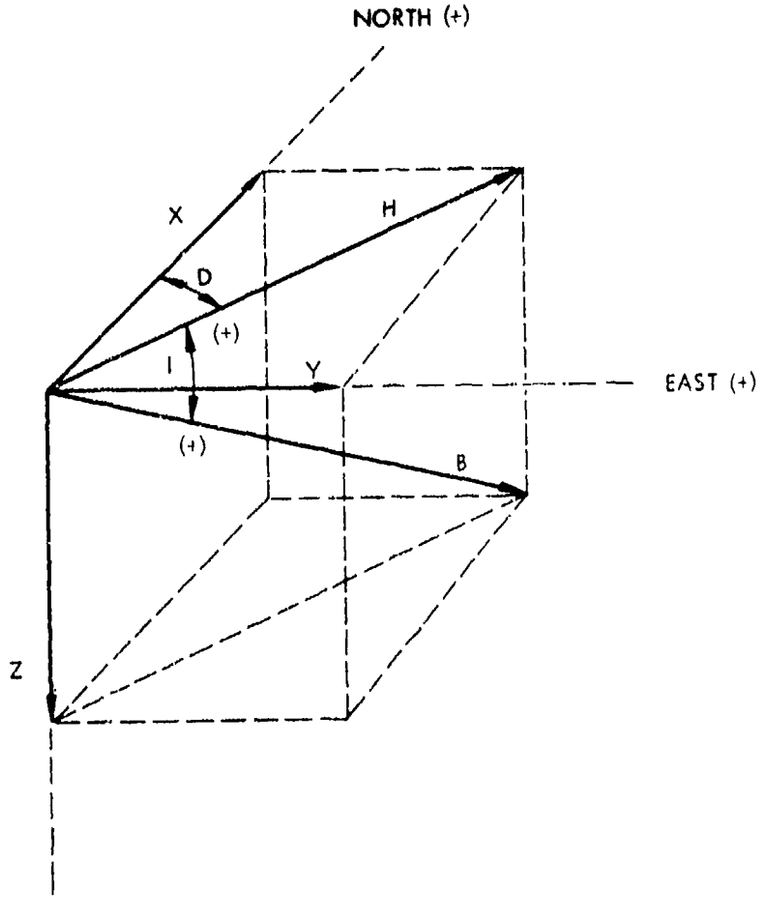

D = DECLINATION
H = HORIZONTAL INTENSITY
B = TOTAL INTENSITY
I = INCLINATION
Z = VERTICAL COMPONENT
X = NORTH COMPONENT
Y = EAST COMPONENT

Figure 2-1. Geodetic elements of the geomagnetic field.

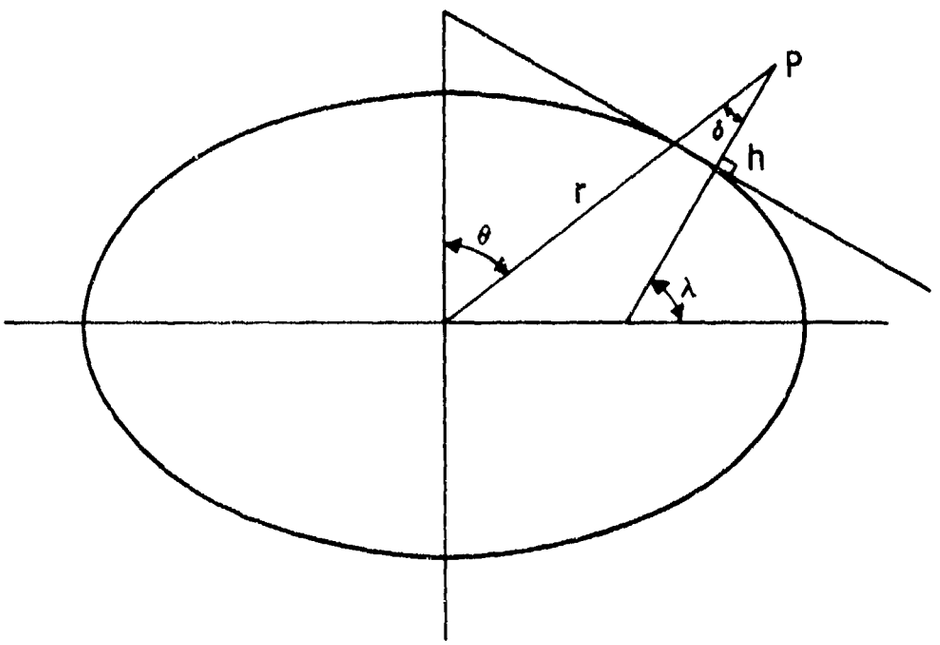

Figure 2-2. Exaggerated ellipse illustrating the geocentric coordinates r, θ, and the geodetic latitude, λ, and altitude, h, of a point P. (δ is the rotational angle between the geocentric and geodetic vectors (B_θ, B_r) and (X, Z), respectively.)

The expressions relating these quantities are thus

$$B_\theta = -X \cos\delta + Z \sin\delta$$

$$B_\varphi = -Y$$

$$B_r = -Z \cos\delta - X \sin\delta$$

where the maximum value of δ is about 0.2 degree.

The magnetic declination D is the angle between X and the horizontal intensity component H, and is given by the deviation of a compass from true north. A positive declination results from an eastward deviation. The inclination, or dip angle I, is the angle between H and B and is given by the dipping of a magnetic needle below the horizontal plane. The dip angle has a positive sense when directed downward.

Routine observations of the absolute field intensity and its temporal variations are made at over 100 permanent magnetic observatories distributed almost entirely on the major continents. Organized attempts have been made periodically to resurvey the field and to check secular variation by reoccupying "repeat stations." Since most surface or aircraft surveys are too slow (and expensive) to take a crisp "snapshot" at the field before secular change can blur the picture, plans are underway for a satellite vector survey about 1980. The last series of satellite surveys were of total field only and covered the epochs 1964-1971.

To completely specify the field vector at an isolated point requires the measurement of three independent elements of the field. For example, B, D, and I are routinely measured aboard the U.S. Navy's project MAGNET aircraft which has supplied most of the global survey data for the past two decades. Fixed observatories usually observe D, H, and Z.

Figures 2-3 and 2-4 show the surface magnetic field elements B and I for epoch 1965. These charts show isomagnetic lines along which the respective geomagnetic field elements are constant. Such charts as these are generally projections or "forecasts" of the field made on the basis of data taken prior to the published epoch and are thus not always of definitive accuracy, nor can they be extrapolated forward in time without error because of the secular variation which is only partly predictable. Because of the sparsity of recent data in remote or communist-controlled areas, some of the vector data used in preparing such charts as these were taken several decades ago.

The secular variation in total intensity averaged over the interval 1965-1970 from POGO satellite data is given in Figure 2-5. There are now indications that the secular variations in B over portions of Asia and the Indian Ocean have already changed significantly from that represented here.

2.3 THE DIPOLAR FIELD OF THE EARTH

The simplest approximation to the geomagnetic field is the field that would result from an Earth-centered dipole directed southward and inclined at 11.5 degrees to the Earth's rotational axis (north and south poles at 78.5 degrees north, 291 degrees east, and at 78.5 degrees south, 111 degrees east, respectively). An improved approximation is the field that would originate from a dipole displaced 0.0685 Earth radius from the Earth's center toward a direction defined by

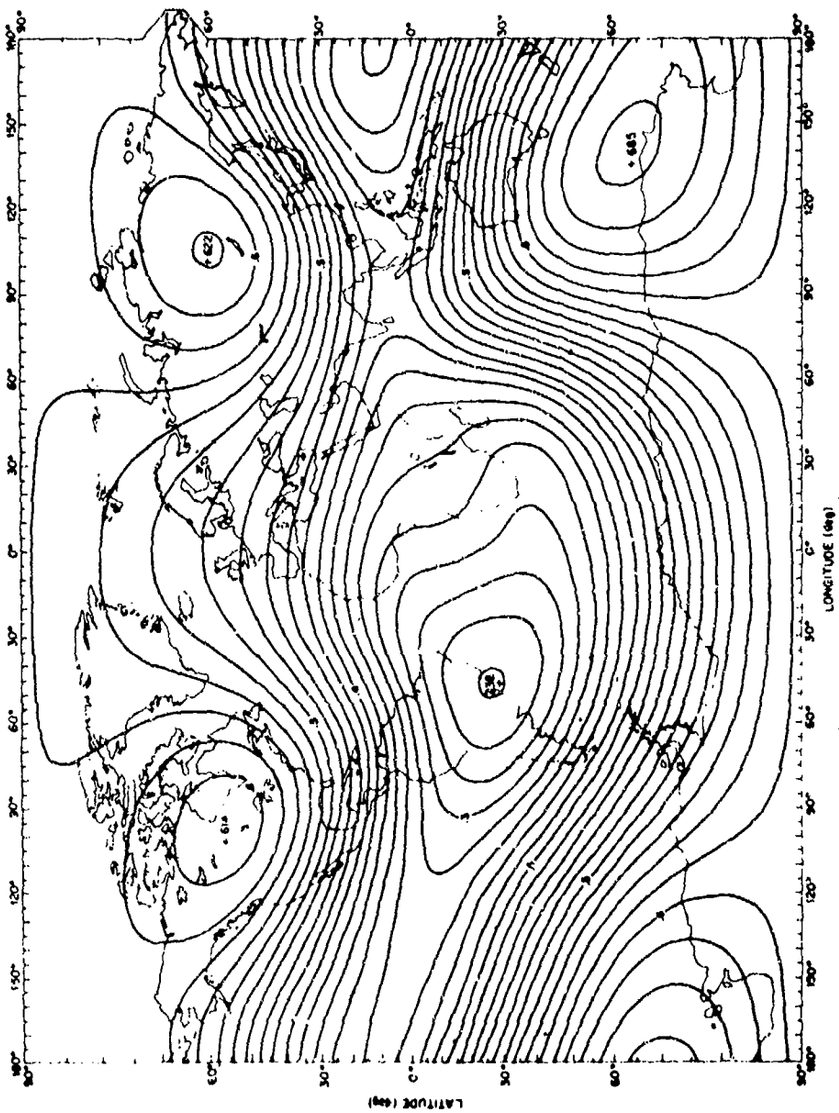

Figure 2-3. Isocontours of surface geomagnetic field intensity B (in gauss) for epoch 1965 (Reference 1).

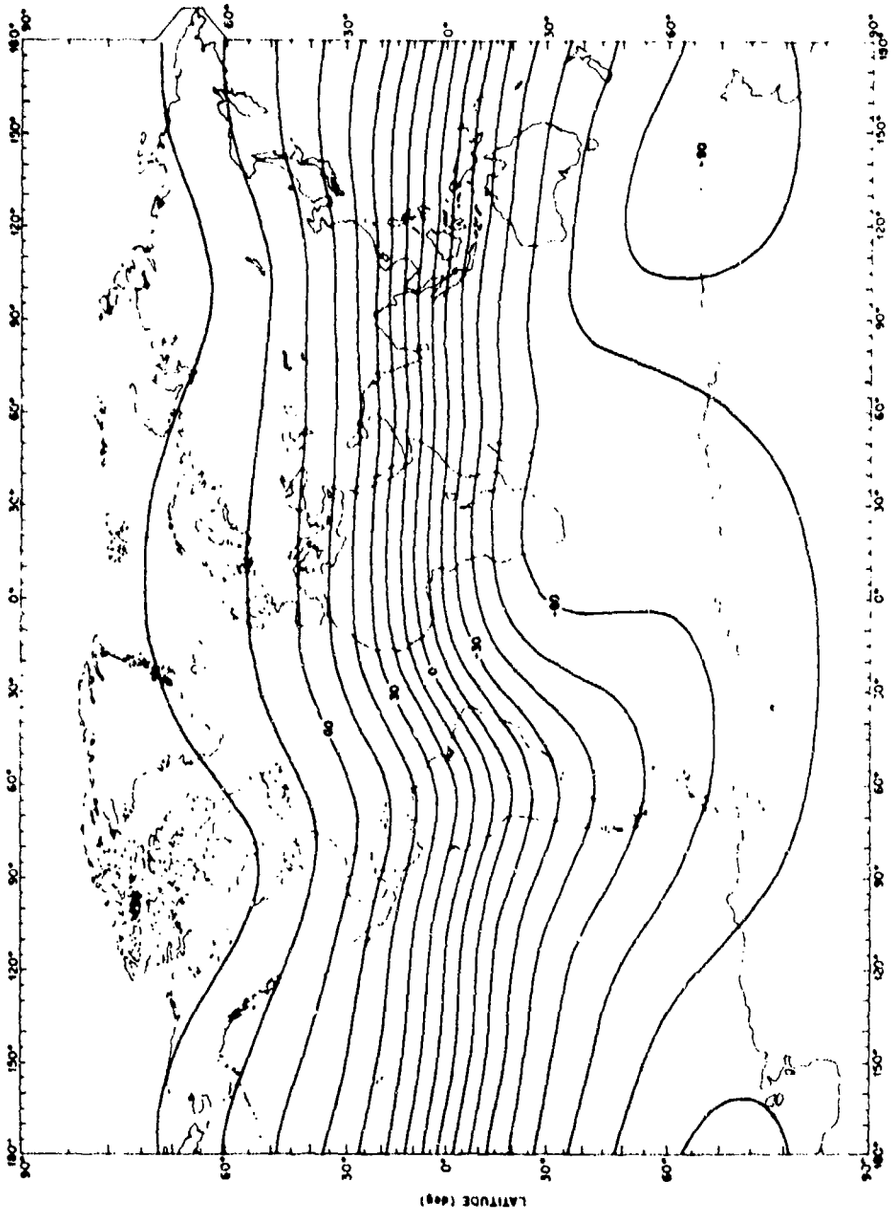

Figure 2-4. Isocontours of magnetic inclination I (in degrees) at the Earth's surface for epoch 1965 (Reference 1).

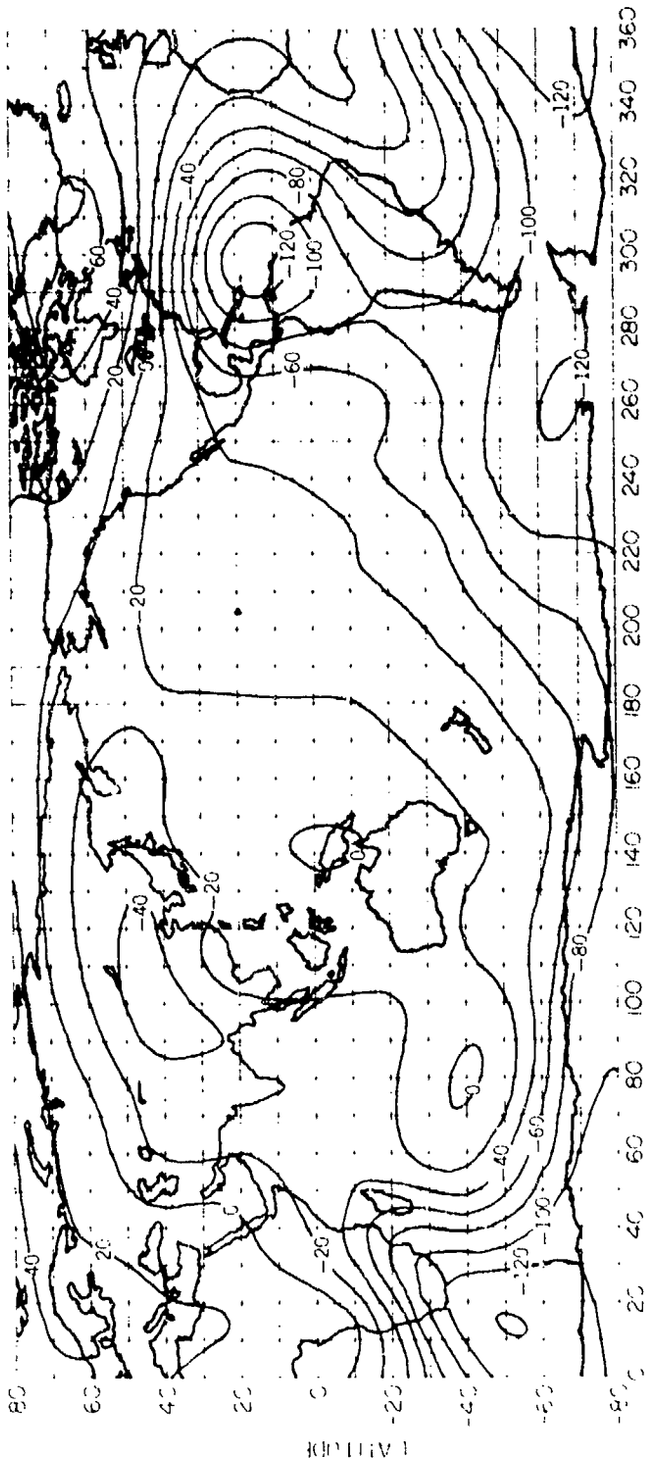

Figure 2-5. Average secular change in total field 1965.7-1970.6, as derived from POGO data (Reference 2). (Contours are in nT/year.)

geographic latitude 15.6 degrees north and longitude 150.9 degrees east. The intersections of the displaced dipole axis with the Earth's surface are at 81.0 degrees north, 84.7 degrees west, and at 75.0 degrees south, 120.4 degrees east (Reference 3). Because the north pole of the magnetic dipole field is located in the southern geographic hemisphere, the sense of the field direction is from south toward north. The field intensity at the equator on the surface is about $B_E \approx 0.312$ gauss (Reference 4).

A simple dipole field has these components (Reference 5) in a spherical coordinate system:

$$B_r = \frac{2M}{r^3}\cos\theta = 2B_o\left(\frac{R_o}{r}\right)^3\cos\theta \qquad (2\text{-}1a)$$

$$B_\theta = \frac{M}{r^3}\sin\theta = B_o\left(\frac{R_o}{r}\right)^3\sin\theta \qquad (2\text{-}1b)$$

whereas the dipole field in a cylindrical coordinate system has the following coordinates:

$$B_R = -\frac{3MRz}{\left(R^2+z^2\right)^{5/2}} \qquad (2\text{-}2a)$$

$$B_z = +\frac{M(R^2-2z^2)}{\left(R^2+z^2\right)^{5/2}} \qquad (2\text{-}2b)$$

The magnetic moment (M) of the Earth's field is approximately $M_E \approx -8.07 \times 10^{25}$ gauss $cm^3 \approx 0.312$ gauss (Earth radii)^3. The magnetic field at the equator, where $R = r = R_o$, is denoted by B_o. The components of the Earth's field are illustrated on Figures 2-6 and 2-7 (south is in the -z direction).

The intensity of a magnetic field is the vector sum of its components; in spherical coordinates

$$B = \sqrt{B_r^2 + B_\theta^2} = \frac{M}{r^3}\sqrt{1+3\cos^2\theta} \qquad (2\text{-}3)$$

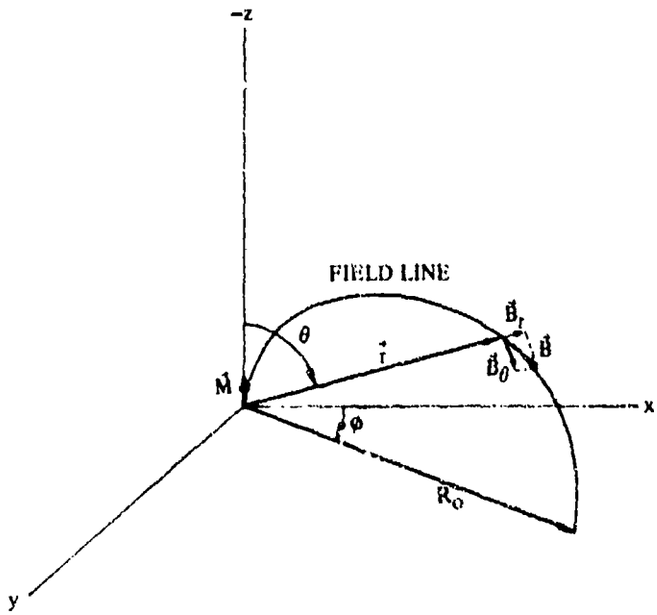

Figure 2-6. A magnetic dipole field in spherical coordinates.

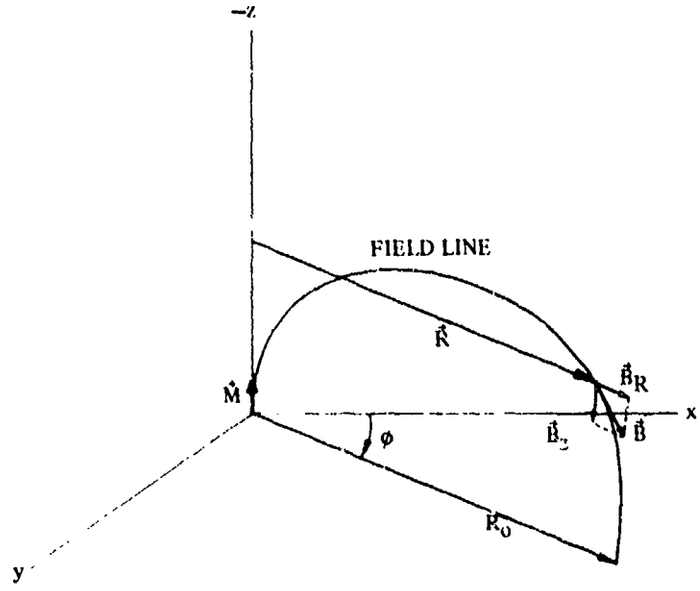

Figure 2-7. A magnetic dipole field in cylindrical coordinates.

and in cylindrical coordinates

$$B = \sqrt{B_R^2 + B_z^2} = M \sqrt{\frac{R^2 + 4z^2}{\left(R^2 + z^2\right)^4}} \quad . \tag{2-4}$$

The field lines, which have everywhere the direction of the vector $\overline{B}$, are defined by the following equations. In spherical coordinates

$$r = R_o \sin^2\theta \tag{2-5}$$

and in cylindrical coordinates

$$R^2 R_o = \left(R^2 + z^2\right)^{3/2} \quad . \tag{2-6}$$

One-half of a field line is illustrated on Figures 2-6 and 2-7. Several representative field lines are shown on Figure 2-8 along with contours of equal field intensity. Each field line is labeled according to its equatorial intersection $R_o = LR_E$. The constant-B curves are equivalent to:

$$B = \frac{0.312}{L^3} \sqrt{\frac{1 + 3\sin^2\lambda}{\cos^6\lambda}} \quad .$$

Numerical magnitudes correspond to the Earth's field. When the constant-B curves are rotated about the polar axis, the result is a closed, egg-shaped constant-B surface (see Figure 3-11). R_E is the radius of the Earth, λ is latitude, and L corresponds to the magnetic shell parameter in Reference 6.

2.3.1 Distance Along Field Line and Volume Between Shells of Field Lines

The distance (S) measured along a field line from the equator is a useful parameter and is sometimes used to identify a point on a field line. As a function of $\xi = \sin\lambda \cos\theta$, the differential distance element for a dipole field is

$$dS = R_o \sqrt{1 + 3\xi^2}\, d\xi \quad . \tag{2-7}$$

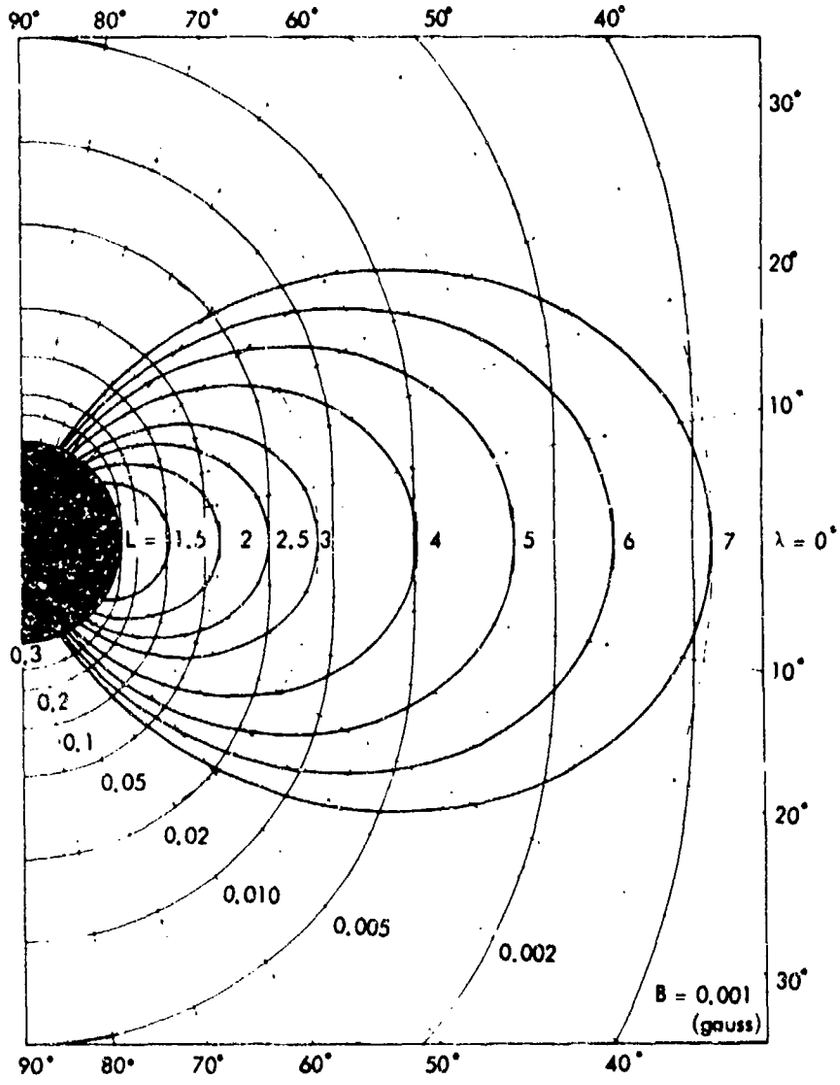

Figure 2-8. Constant-B surfaces in a dipole field.

The integrated distance along a dipole field line from equater to $\xi \sin\lambda$ is:

$$S = \frac{R_o}{2}\left[\xi\sqrt{1+3\xi^2} + \frac{1}{\sqrt{3}}\ln\left(\sqrt{3}\xi + \sqrt{1+3\xi^2}\right)\right] \quad . \qquad (2\text{-}8)$$

S is plotted on Figure 2-9 (in units $R_o = LR_E$) (see Table 3B-1). The scale at the bottom of the figure is the equatorial pitch angle of a particle that mirrors at the corresponding latitude. Up to 50 degrees latitude, S can be determined with fair accuracy by means of the empirical formula:

$$S \approx 0.019\,\lambda\,R_o$$

where λ is expressed in degrees. At 90 degrees latitude, $S = 1.3802\,R_o$.

The derivative of magnetic field intensity along the field line is

$$\frac{dB}{dS} = \frac{B_o}{R_o}\,\frac{3\xi\left(3+5\xi^2\right)}{\left(1-\xi^2\right)^4\left(1+3\xi^2\right)} \quad . \qquad (2\text{-}9)$$

From Equation 2-7, the volume between two cylindrically symmetric shells bounded by dipole field lines is fairly simple to obtain. If the shells are located at an equatorial distance $R_o = R_E L$ and separated by a small distance $\delta R_o = R_E \delta L$, the volume included between the two L shells is:

$$\delta V = 4\pi R_E^3\sqrt{1-\frac{1}{L}}\left[\frac{16}{35}L^3 + \frac{8}{35}L^2 + \frac{6}{35}L + \frac{1}{7}\right]\delta L \quad . \qquad (2\text{-}10)$$

The total volume contained between the Earth's surface and a shell of field lines with an equatorial intersection at R_o is plotted on Figure 2-10 as a function of $L = R_o/R_E$. In these equations, R_E is the radius of the Earth and L corresponds to the magnetic shell parameter of McIlwain (Section 3).

2.3.2 Geomagnetic Coordinate Systems

Various coordinate systems based upon the geomagnetic field are used in place of geographic coordinates to simplify the study of trapped radiation and other phenomena in space that are controlled

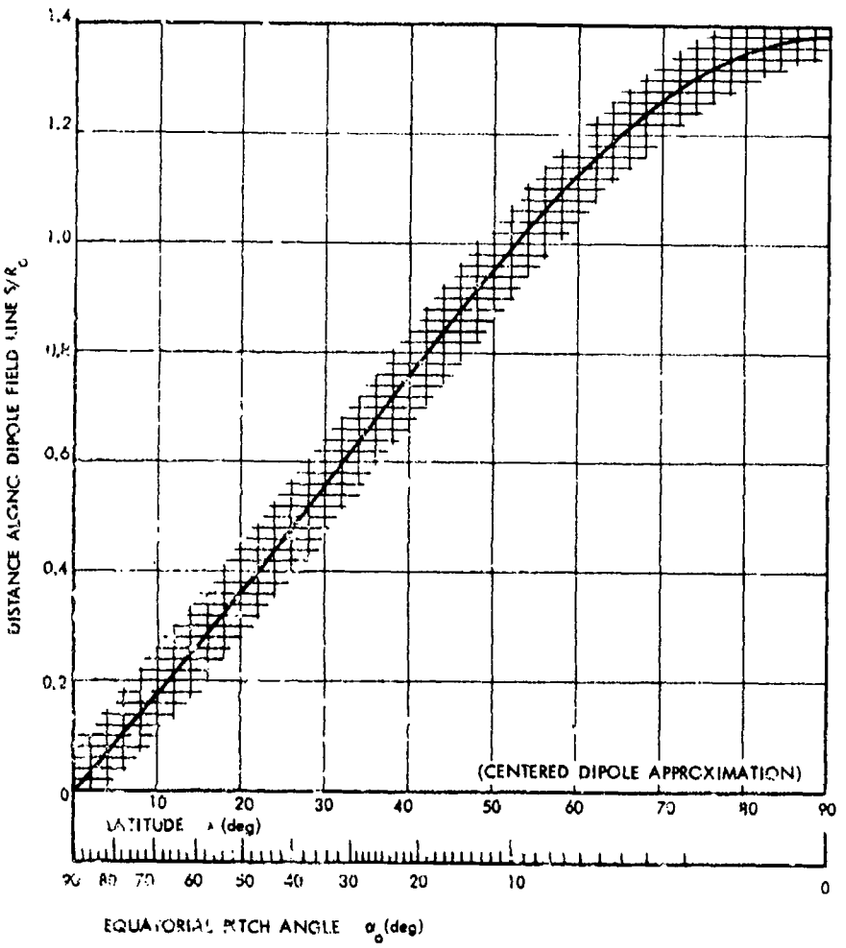

Figure 2-9. Distance along a dipole field line measured from the equator.

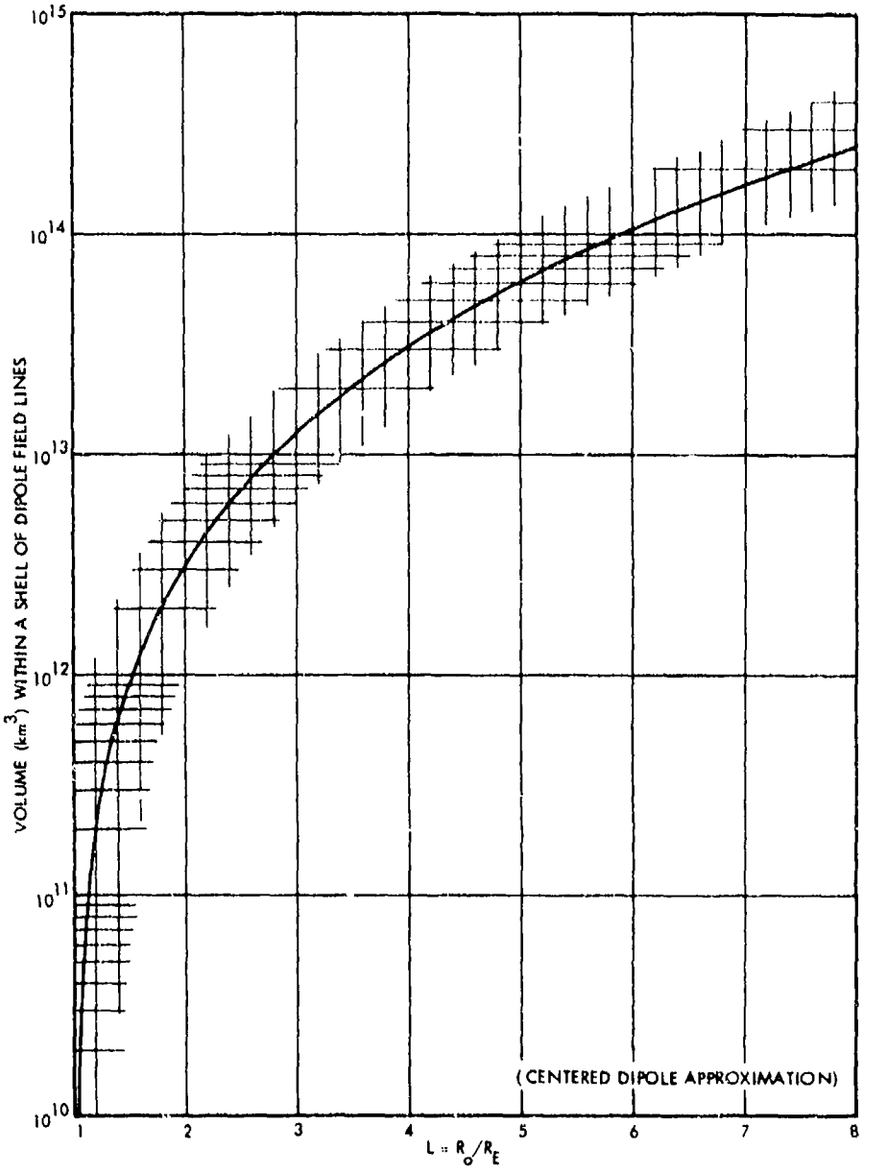

Figure 2-10. Volume contained within a shell of dipole field lines.

or influenced by the field. The most elemental geomagnetic coordinate system is one aligned with the centered dipole. It is shown on Figure 2-11, superimposed on geographic coordinates. The points where the dipole axis intersects the Earth's surface serve to locate the geomagnetic (or dipole) north and south poles (78.5 degrees north, 291 degrees east and 78.5 degrees south, 111 degrees east, respectively). The geomagnetic equator lies in a plane passing through the center of the Earth and perpendicular to the dipole axis.

Angular positions in this system are expressed as geomagnetic (or dipole) latitude and geomagnetic longitude. The prime geomagnetic meridian contains the geographic south pole and lies approximately along the geographic meridian 290 degrees east (70 degrees west) over most of its length. In analogy with the definition of local geographic time, local geomagnetic time is defined in terms of the angular position (in hours) of the Sun relative to the geomagnetic meridian of the observer. Geomagnetic noon occurs when the Sun is in the geomagnetic meridian plane of the observer.

An accurate coordinate system of geomagnetic latitude and geomagnetic longitude [based on the field-line configuration given by the international geomagnetic reference field 80-term expansion (References 7 and 8) for epoch 1969.75] has been prepared in Reference 9. In this system, the latitudes are invariant latitudes (see Equation 2-15) and the meridian surfaces are defined by families of field lines intersecting radial lines in a predetermined equatorial plane. North and south polar plots and world maps of this system of geomagnetic latitude and longitude are provided in Appendix 2B for the surface of the Earth and at a 3,000-kilometer altitude.

A coordinate system of considerable utility is one in which each dipole field line is labeled by the magnetic shell parameter L, R_O/R_E (Reference 6) and a point on the field line is identified by the field intensity B at the point. Sometimes the geomagnetic latitude, the distance S along the field line, or a set of curves defined by:

$$r \quad [\text{constant}] \sqrt{\cos \theta} \quad , \tag{2-11}$$

which are orthogonal to the field lines, are employed instead of B to specify points on the field line.

The analysis of trapped particles is complicated because the geomagnetic field actually has a high degree of azimuthal asymmetry.

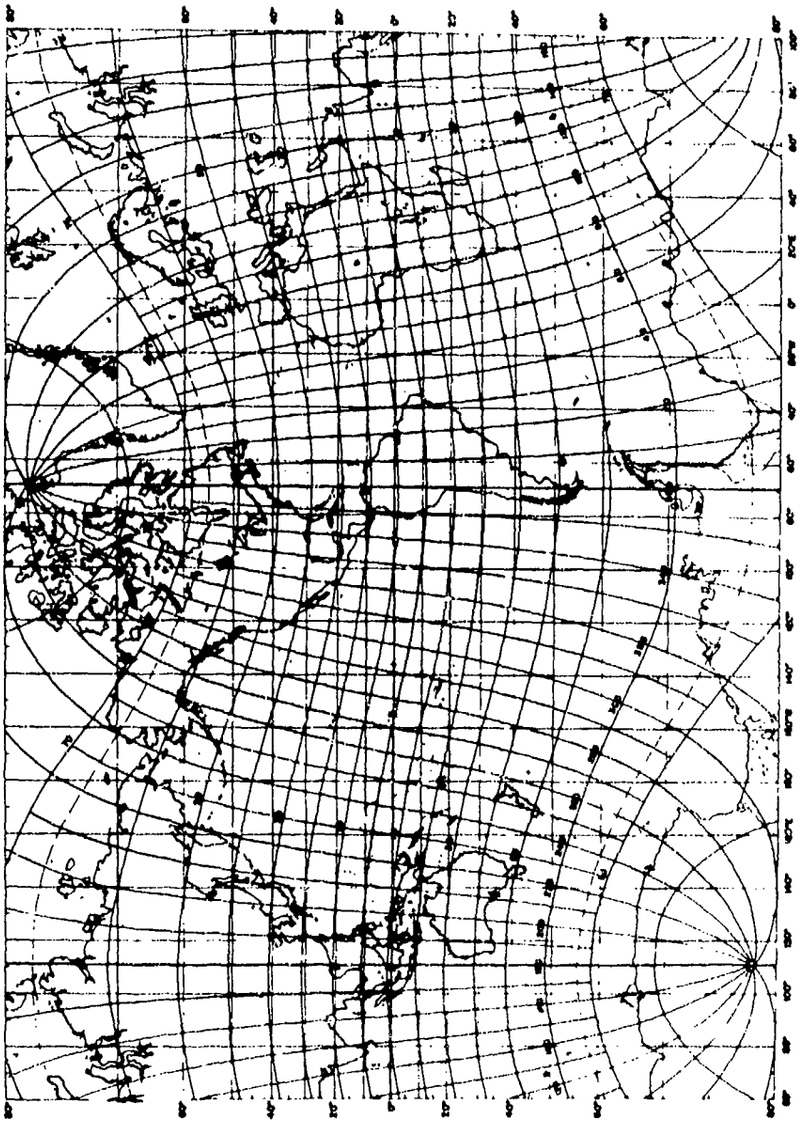

Figure 2-11. Geomagnetic coordinate system given by a centered dipole, superimposed on geographic coordinates (Reference 10).

Symmetric coordinate systems based upon the terrestrial dipole are found to have only limited applicability. Various coordinate systems, based upon parameters analogous to some of those described previously for a dipole field, have been proposed with the intent of restoring some of the aspects of azimuthal symmetry (Reference 6). Trapped particle populations thereby can be described in terms of an idealized dipole field with strict azimuthal symmetry. A discussion of coordinate systems of this kind, which involves equations of motion, is contained in subsection 3.4.3.

2.4 THE SPHERICAL HARMONIC EXPANSION OF THE FIELD

Although the simple dipole approximation is useful in some cases, a higher order approximation generally is required to describe the field in most trapped radiation studies.

With the assumption that electric currents are negligible in the region above the Earth, the magnetic field $\overline{B}$ is caused only by the internal sources of the main field, and can be expressed as the negative gradient of a magnetic potential Ψ_m that satisfies Laplace's equation:

$$\overline{B} = -\nabla\Psi_m \quad . \tag{2-12}$$

The general solution for Ψ_m can be expressed as a sum of spherical harmonics (Reference 11):

$$\Psi_m \cong R_E \sum_{n=1}^{n'} \left(\frac{R_E}{r}\right)^{n+1} \sum_{m=0}^{n} P_n^m(\theta) \left[g_n^m \cos m\phi + h_n^m \sin m\phi\right] ; \; r \geq R_E \tag{2-13}$$

where r is the radial distance from the Earth's center, R_E is the Earth's radius, and θ and ϕ are geographic colatitude and east longitude, respectively. The Schmidt functions (Reference 11):

$$P_n^m(\theta) = \left[\frac{(n-m)!\left(2-\delta_{o,m}\right)}{(n+m)!}\right]^{1/2} P_{n,m}(\theta) \tag{2-14}$$

are multiples of the associated Legendre functions $P_{n,m}(\theta)$ of degree n and order m; the Kronecker delta ($\delta_{o,m}$) equals one if m = 0 and equals zero if $m \neq 0$. The g_n^m and h_n^m are constants referred to as Gaussian coefficients whose values (to some maximum n') are obtained from a best fit to measured values of the magnetic field (Equation 2-12). Once the g_n^m and the h_n^m are known, Ψ_m is determined and defines the field for $r \geq R_E$. Analytic techniques have been developed recently that allow Gaussian coefficients to be derived from measured values of the total field intensity rather than from measured field components (Reference 12), thus making possible the utilization of numerous satellite measurements. These coefficients are also expanded in a linear or higher order series in time to allow for secular change.

Ψ_m is sometimes expanded in Gauss-normalized, associated-Legendre functions (Reference 11) rather than in Schmidt-normalized functions. Either representation is valid, of course, but some practical value exists in using Schmidt functions since the magnitudes of the corresponding g_n^m and h_n^m then will indicate the relative contribution of the various terms in the series.

The assumption that electric currents are absent in the ionosphere is, of course, only an approximation since field-aligned currents are almost always present in polar regions, and the dayside ionosphere contains the Sq system. These effects contribute up to a few hundred nanotesla under active conditions in polar regions, and up to 20 to 100 nanotesla at the magnetic equator, depending upon the altitude above the E-layer.

2.4.1 Field Models

Tables of Gaussian coefficients have been determined by a number of investigators. The field models that have been applied to trapped radiation studies, or might be considered for the present, are:

1. The Jensen and Whitaker (JW) 569-coefficient model (Reference 13) epoch 1955.
2. The Jensen and Cain (JC) 48-coefficient model (Reference 14) epoch 1960.
3. The Goddard Space Flight Center (GSFC (9/65)) 99-coefficient model (Reference 15) epoch 1965.

4. The Goddard Space Flight Center (GSFC (12/66)) 120-coefficient model (Reference 16) epoch 1965.
5. The International Geomagnetic Reference Field (IGRF) 80-coefficient model (References 17, 18) epoch 1965.
6. The Institute for Geological Sciences (IGS) 168-coefficient model (Reference 19) epoch 1975.
7. The American World Chart (AWC) 168-coefficient model (Reference 20) epoch 1975.

Except for JW and IGRF, these various models have been derived by fitting observed surface and satellite magnetic survey data. The JW model, used for reducing Explorer 4 data, was a very precise fit to the 1955 U.S. magnetic charts of the vertical component. It was later found that these charts were relatively inaccurate. The JC model, although having fewer terms and no time derivatives, was a better measure of the field for (and previous to) its 1960 epoch. It was thus widely used in interpreting trapped radiation data. The later GSFC models contain more coefficients and thus are better representations of the low-altitude field.

The IGRF model (epoch 1965) was derived as a weighted average of candidate models and is fairly accurate for the interval 1960 to 1968. An IGRF model for 1975 has been recently derived (Reference 21). The coefficients for this model are listed in Table 2-1. One of the best models for epoch 1975 is the IGS model (Reference 19), although its use of parabolic terms makes it unlikely that an extrapolation over epochs 1975-1980 is wise. It is not clear whether the IGS, using, say, its linear secular terms only, or the AWC model (Reference 20) is the preferred representation for current epochs.

Both of the latter models have set their epochs at 1975.0 for the convenience of users and to imply that an attempt has been made to represent the current field. However, neither model actually included much data later than about 1972, and, thus, the choice only can be made by comparison with recent data.

2.4.2 B, L Coordinates

The charts in Appendix 2C show contours of the total field intensity at various altitudes, as determined from the Jensen and Cain field model. Tables of coordinate points defining geomagnetic field lines are given in Reference 22 for a representative group of field lines distributed around the Earth.

Table 2-1. IGRF 1975 coefficients (Reference 21). (The coefficients are Schmidt normalized.)

n	m	Main Field, nT		Secular Change, nT/yr	
		g	h	$\dot{g}$	$\dot{h}$
1	0	-30,186		25.6	
1	1	-2,036	5735	10.0	-10.2
2	0	-1,898		-24.9	
2	1	2,997	-2124	0.7	-3.0
2	2	1,551	-37	4.3	-18.9
3	0	1,299		-3.8	
3	1	-2,144	-361	-10.4	6.9
3	2	1,296	249	-4.1	2.5
3	3	805	-253	-4.2	-5.0
4	0	951		-0.2	
4	1	807	148	-2.0	5.0
4	2	462	-264	-3.9	0.8
4	3	-393	37	-2.1	1.7
4	4	235	-307	-3.1	-1.0
5	0	-204		0.3	
5	1	368	39	-0.7	1.2
5	2	275	142	1.1	2.3
5	3	-20	-147	-1.6	-2.0
5	4	-161	-99	-0.5	1.3
5	5	-38	74	1.0	1.1
6	0	46		0.2	
6	1	57	-23	0.5	-0.5
6	2	15	102	2.0	-0.1
6	3	-210	88	2.8	-0.2
6	4	-1	-43	0.0	-1.3
6	5	-8	-9	0.9	0.7
6	6	-114	-4	-0.1	1.7
7	0	66		0.0	
7	1	-57	-68	0.0	-1.4
7	2	-7	-24	0.0	-0.1
7	3	7	-4	0.6	0.3
7	4	-22	11	0.9	0.3
7	5	-9	27	0.3	-0.7
7	6	11	-17	0.3	0.1
7	7	-8	-14	-0.5	0.8
8	0	11		0.2	
8	1	13	4	0.3	-0.2
8	2	3	-15	0.0	-0.4
8	3	-12	2	0.2	-0.2
8	4	-4	-19	-0.4	-0.3
8	5	6	1	-0.3	0.4
8	6	-2	18	0.6	-0.3
8	7	9	-6	-0.3	-0.6
8	8	1	-19	-0.1	0.3

The charts in Appendix 2C also show contours of constant L, where L is the parameter associated with a magnetic shell (Reference 6) in the geomagnetic field and is analogous to the $L = R_O/R_E$ defined for a dipole field in subsection 2.3.2. L is discussed in detail in Section 3.

A coordinate system employing B and the parameter L is used extensively to describe the distribution of trapped particles in radiation belts. Because of the azimuthal asymmetry of the geomagnetic field, the altitude of a constant B, L contour around the Earth will vary with longitude. Figure 2-12 shows the variation for several values of B on the magnetic shell L = 1.20. B is in gauss. The curves are based upon the field model in Reference 14. Similar graphs are also given in Appendix 2D for L = 1.12, 1.60, 2.20, and 3.50. These graphs are useful because trapped particles experience similar changes in their mirror point altitudes as they drift around the Earth. (Trapped particle motion is discussed in Section 3.)

For the cases shown, the variations in altitude are appreciable; maximum variations of 1,200 to 1,500 kilometers occur in the southern hemisphere. The minimum altitude for a given value of B is observed to occur in the southern hemisphere near 315 degrees east longitude. More precisely, the minimum altitudes occur in the southern Atlantic near Brazil in a region of low field values (Figure 2-3) known variously as the South American, South Atlantic, or Brazilian anomaly. However, this feature of the geomagnetic field is not really anomalous, but is just the result of the field lines dipping closer to the Earth in the anomaly region because of the eccentricity of the geomagnetic field with respect to the Earth's center.

The South American anomaly is important in trapped radiation studies because it is a region in which particle losses caused by atmospheric scattering are enhanced as a consequence of the denser atmosphere encountered by the particles as they move through their minimum altitudes. A comprehensive graph of minimum altitudes in the anomaly as a function of B and L is presented on Figure 2-13. Particle measurements in the B, L regions below 1,000 kilometers should show solar cycle effects because of changes in atmospheric density and composition.

For easy visualization, fluxes in B, L space are sometimes transformed to polar coordinate space r, λ defined by the dipole relations (Reference 6). Figure 2-14 is a mapping of polar coordinates onto the B, L plane by means of the dipole relations:

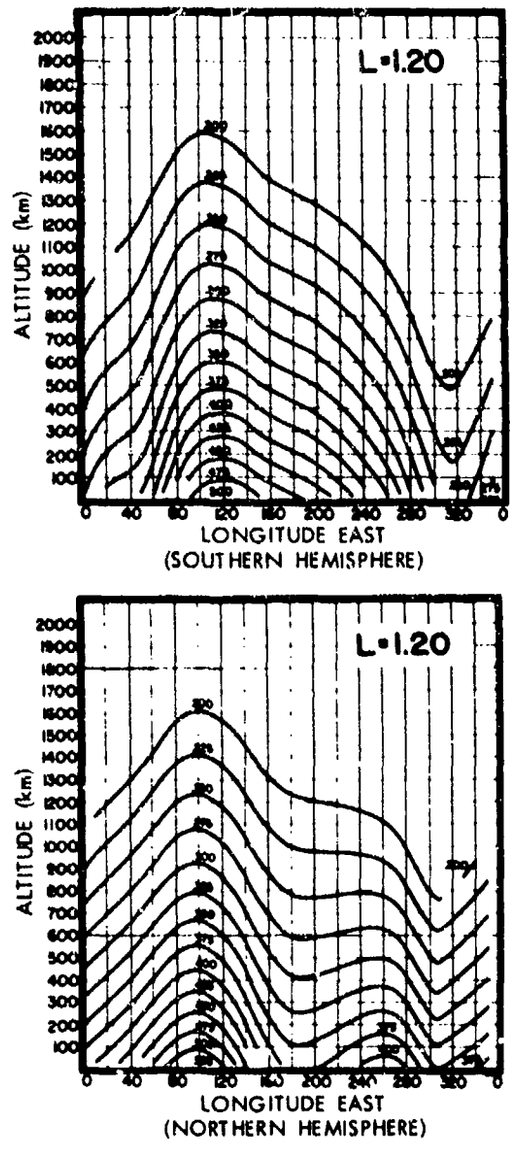

Figure 2-12. Altitude versus longitude for constant-B traces on the magnetic shell L = 1.20 (Reference 23).

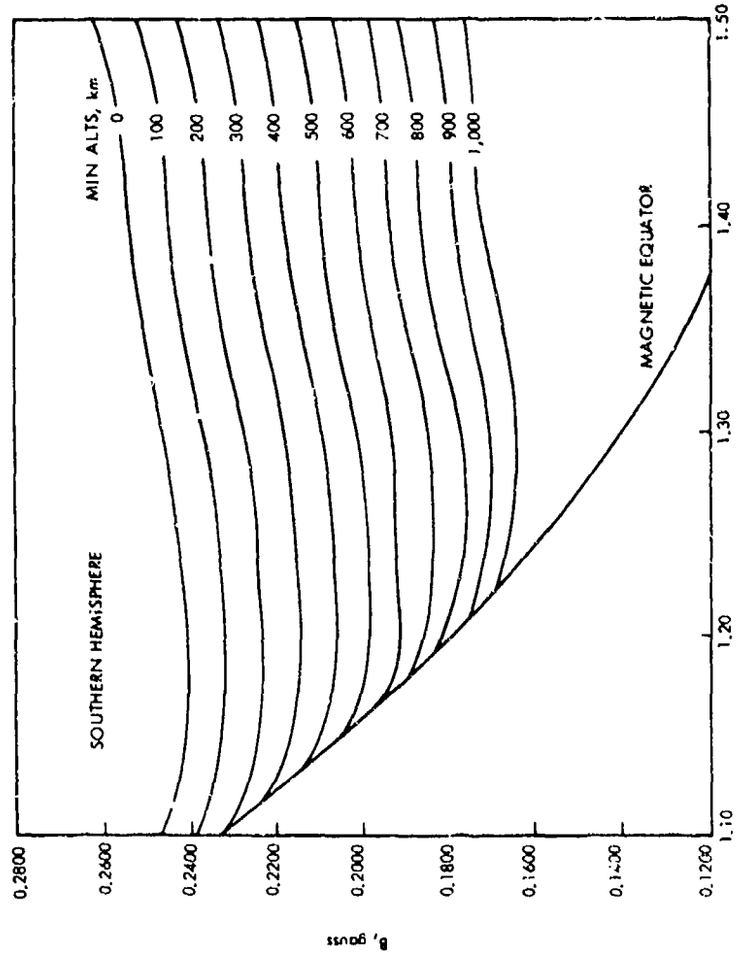

Figure 2-13. Values of minimum altitudes in the southern hemisphere as a function of B, L.

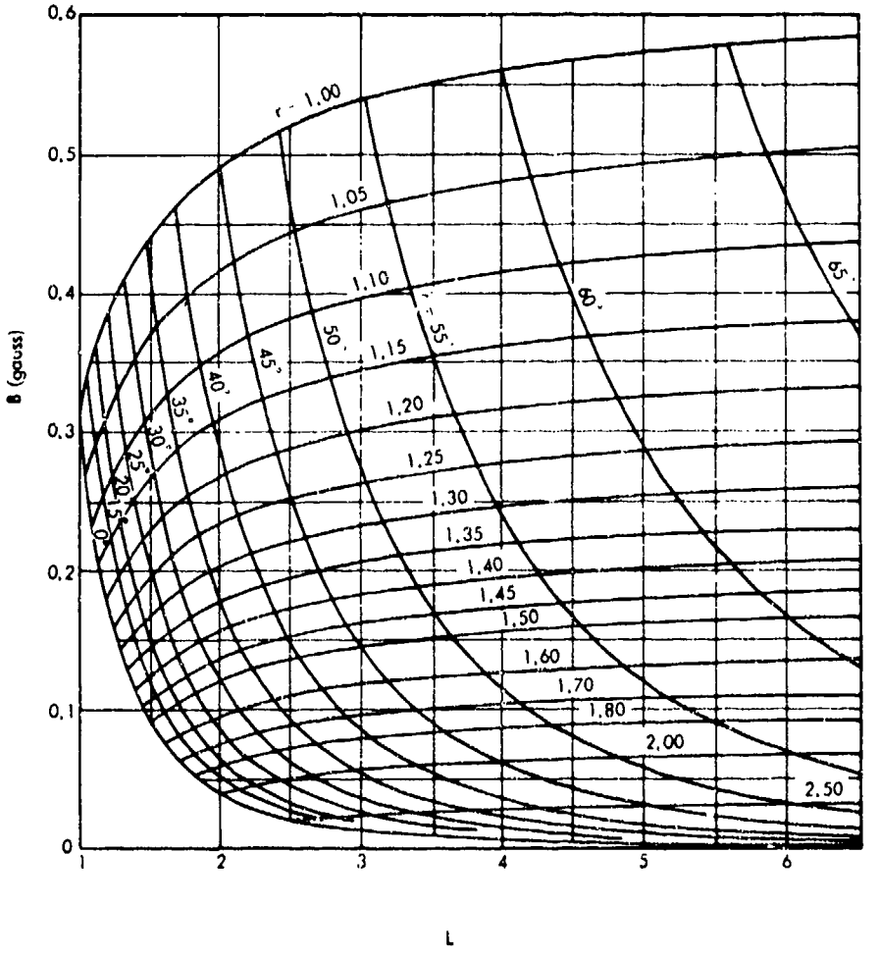

Figure 2-14. Mapping of the r, λ coordinates onto the B, L plane by means of the dipole relations.

$$B = \frac{0.312}{r^3}\left(4 - \frac{3r}{L}\right)^{1/2}, \quad r = L\cos^2\lambda \quad .$$

In these relations, r is expressed in units of Earth radii. At low values of λ, determining numerical values from Figure 2-8 might be preferable. Some caution should be exercised in using the figure because of the asymmetry of the geomagnetic field.

The invariant latitude (Λ) defined by the expression:

$$\cos^2\Lambda = 1/L \qquad (2\text{-}15)$$

is sometimes used to organize auroral or particle precipitation data near Earth. It is interpreted as the latitude where the magnetic shell, whose value is L, intersects the Earth. Table 2-2 gives values of Λ versus L for 0.5-degree intervals in Λ from 0 to 89.5 degrees.

2.4.3 Computer Codes for $\overline{B}$ and L

Over the past decades, several different computer codes have been developed for the prediction of both $\overline{B}$ and L. Those based upon spherical harmonics were derived from the original formulations of Jensen and Whitaker (for $\overline{B}$) and McIlwain (for L) and bear such names as GFIELD, FIELD, SPHRC, INVAR, etc. (see subsection 11.4). Copies of these can be obtained from either the National Space Sciences Data Center (Goddard), the NOAA Data Center (Boulder), or the U.S. Geological Survey (Denver). Tradeoffs of speed, core size, and flexibility can be evaluated for the particular application.

A different formulation for the computation of $\overline{B}$ and L has been developed by B. Kluge (Reference 24) at ESRO/Darmstadt. This formulation, which employs a mapping of the field in 1/r space, has no advantage over the spherical harmonic developments for $\overline{B}$. However, for the calculation of L, a table is provided from which a much faster L computation can be made than with the McIlwain integration program. The only drawback, which is not significant for most applications, is that the tables become fairly large when computations are done for several epochs. The tables must be developed by a careful (Chebychev) fit for each new model.

Table 2-2. Tabular values of invariant latitude Λ (degrees) versus L.

Λ	L	Λ	L	Λ	L	Λ	L
.0	1.0000	22.5	1.1716	45.0	2.0000	67.5	6.8284
.5	1.0001	23.0	1.1802	45.5	2.0355	68.0	7.1261
1.0	1.0003	23.5	1.1891	46.0	2.0723	68.5	7.4447
1.5	1.0007	24.0	1.1982	46.5	2.1105	69.0	7.7865
2.0	1.0012	24.5	1.2077	47.0	2.1500	69.5	8.1536
2.5	1.0019	25.0	1.2174	47.5	2.1910	70.0	8.5486
3.0	1.0027	25.5	1.2275	48.0	2.2335	70.5	8.9745
3.5	1.0037	26.0	1.2379	48.5	2.2776	71.0	9.4344
4.0	1.0049	26.5	1.2486	49.0	2.3233	71.5	9.9322
4.5	1.0062	27.0	1.2596	49.5	2.3709	72.0	10.4721
5.0	1.0077	27.5	1.2710	50.0	2.4203	72.5	11.0590
5.5	1.0093	28.0	1.2827	50.5	2.4716	73.0	11.6985
6.0	1.0110	28.5	1.2948	51.0	2.5250	73.5	12.3970
6.5	1.0130	29.0	1.3073	51.5	2.5805	74.0	13.1621
7.0	1.0151	29.5	1.3201	52.0	2.6383	74.5	14.0024
7.5	1.0173	30.0	1.3333	52.5	2.6984	75.0	14.9282
8.0	1.0198	30.5	1.3470	53.0	2.7610	75.5	15.9515
8.5	1.0223	31.0	1.3610	53.5	2.8263	76.0	17.0864
9.0	1.0251	31.5	1.3755	54.0	2.8944	76.5	18.3497
9.5	1.0280	32.0	1.3905	54.5	2.9655	77.0	19.7617
10.0	1.0311	32.5	1.4059	55.0	3.0396	77.5	21.3465
10.5	1.0344	33.0	1.4217	55.5	3.1171	78.0	23.1335
11.0	1.0378	33.5	1.4381	56.0	3.1980	78.5	25.1588
11.5	1.0414	34.0	1.4550	56.5	3.2826	79.0	27.4664
12.0	1.0452	34.5	1.4724	57.0	3.3712	79.5	30.1116
12.5	1.0491	35.0	1.4903	57.5	3.4639	80.0	33.1634
13.0	1.0533	35.5	1.5088	58.0	3.5611	80.5	36.7098
13.5	1.0576	36.0	1.5279	58.5	3.6629	81.0	40.8634
14.0	1.0622	36.5	1.5475	59.0	3.7698	81.5	45.7716
14.5	1.0669	37.0	1.5678	59.5	3.8821	82.0	51.6285
15.0	1.0718	37.5	1.5888	60.0	4.0000	82.5	58.6955
15.5	1.0769	38.0	1.6104	60.5	4.1240	83.0	67.3304
16.0	1.0822	38.5	1.6327	61.0	4.2546	83.5	78.0337
16.5	1.0877	39.0	1.6558	61.5	4.3921	84.0	91.5231
17.0	1.0935	39.5	1.6795	62.0	4.5371	84.5	108.8564
17.5	1.0994	40.0	1.7041	62.5	4.6902	85.0	131.6461
18.0	1.1056	40.5	1.7295	63.0	4.8518	85.5	162.4476
18.5	1.1120	41.0	1.7557	63.5	5.0228	86.0	205.5089
19.0	1.1186	41.5	1.7827	64.0	5.2037	86.5	268.3177
19.5	1.1254	42.0	1.8107	64.5	5.3955	87.0	365.0896
20.0	1.1325	42.5	1.8397	65.0	5.5989	87.5	525.8820
20.5	1.1398	43.0	1.8696	65.5	5.8150	88.0	821.0345
21.0	1.1474	43.5	1.9005	66.0	6.0447	88.5	1459.3566
21.5	1.1552	44.0	1.9326	66.5	6.2893	89.0	3283.1318
22.0	1.1632	44.5	1.9657	67.0	6.5500	89.5	13131.4805

2.5 DISTANT MAGNETIC FIELD

2.5.1 The Need for a Quantitative Description of the Magnetospheric Magnetic Field

The magnetic field at geocentric distances greater than about four Earth radii is distorted by the fields associated with currents flowing in the Earth's magnetosphere. The Earth's main magnetic field (of internal origin), $\overline{B}_{gm}$, interacts with solar wind particles to form several other currents which flow through the Earth's magnetosphere. These current systems and their combined associated magnetic fields, $\overline{B}_{ms}$, deform the geomagnetic field at great altitudes and dominate the magnetic field at altitudes of a few Earth radii. The main contributions to the magnetospheric magnetic field come from the magnetopause currents, the currents which flow across the tail of the magnetosphere, and the ring current of charged particles trapped in the inner magnetosphere.

The magnetopause currents are produced directly by the interaction of the geomagnetic field with the solar wind. Solar wind ions (mostly protons) and electrons are deflected in opposite directions upon encountering the geomagnetic field, giving rise to the magnetopause current system. The resulting field topology is such that it is possible for charged particles to enter and flow across the anti-solar portion of the magnetosphere. This second current system is commonly referred to as the tail current. Particles trapped in the inner magnetosphere form the third current system. The magnetopause and tail current systems are influenced greatly by changes in the interplanetary magnetic field and other interplanetary parameters. The tail magnetic field, in particular, changes during the lifetime of a magnetospheric substorm. These substorms occur typically every several hours and the resulting time-varying magnetic and electric fields serve also to inject particles into the ring current. The ring current is greatly enhanced during magnetic storms by the continuous injection of tail particles.

To accurately represent charged particle phenomena, it is necessary to quantitatively describe the magnetic field ($\overline{B}_{gm} + \overline{B}_{ms}$) in which these particles are found. Above about 60 degrees magnetic latitude, all magnetic field lines extend several Earth radii into space. Therefore, along at least a portion of these field lines their accurate quantitative description necessitates the inclusion of the contribution to the total magnetic field from the three magnetospheric current systems just described. There have been several quantitative model descriptions of the magnetospheric magnetic field. For

a detailed comparison of the more recent ones, see the review by Walker (Reference 25). These models can be tested directly by comparisons with the observed field (as detected with magnetometers and barium cloud traces) and indirectly with charged particle data. Such comparisons indicate (Reference 25) that the Olson-Pfitzer model currently best represents the observed average magnetospheric magnetic field, $\overline{B}_{ms}$. This model is described in subsection 2.5.2.

2.5.2 Description of Olson-Pfitzer Magnetospheric Magnetic Field Model

The Olson-Pfitzer model provides a quantitative description of the total magnetospheric magnetic field (produced by the magnetopause, tail, and quiet-time ring currents). It is to be added to the main magnetic field with appropriate coordinate transformations. This model is semiempirical and contains both basic physics and observational data. It was constructed to quantitatively represent the quiet-time magnetospheric magnetic field for the case of perpendicular incidence of the solar wind onto the geomagnetic field. It currently does not include the effects of the continuously changing angle between the geomagnetic dipole axis and the solar wind direction and, more importantly, magnetic storm effects. Actually, two models have been published. One is the sixth-order-power series expansion with exponential terms and the second is an abbreviated version containing only quadratic terms. In both cases, series expansions are input to a fitting routine which constructs an orthonormal function set in order to fit the input data.

Components of $\overline{B}$ in the sixth-order model are represented as

$$B_x = \sum_{i=0}^{6} \sum_{j=0}^{3} \sum_{k=0}^{3} \left[a_{ijk} + b_{ijk} \exp(-0.03r^2)\right] x^i y^{2j} z^{2k+1} \qquad (2\text{-}16a)$$

$$B_y = \sum_{i=0}^{6} \sum_{j=0}^{3} \sum_{k=0}^{3} \left[c_{ijk} + d_{ijk} \exp(-0.03r^2)\right] x^i y^{2j} z^{2k+1} \qquad (2\text{-}16b)$$

$$B_z = \sum_{i=0}^{6} \sum_{j=0}^{3} \sum_{k=0}^{3} \left[e_{ijk} + f_{ijk} \exp(-0.015r^2)\right] x^i y^{2j} z^{2k} \qquad (2\text{-}16c)$$

$$a_{ijk} = b_{ijk} = 0 \qquad i + 2j + 2k > 6 \qquad (2\text{-}17a)$$

$$c_{ijk} = d_{ijk} = 0 \qquad i + 2j + 2k > 5 \qquad (2\text{-}17b)$$

$$e_{ijk} = f_{ijk} = 0 \qquad i + 2j + 2k > 7 \quad . \qquad (2\text{-}17c)$$

The non-zero coefficients given in Tables 2-3, 2-4, and 2-5 are for the components of the combined ring and tail fields, the magnetopause field, and the total ring plus tail plus magnetopause field, respectively. The point where $\overline{B}_{ms}$ is to be computed is specified by x, y, and z (given in Earth radii). The distance

$$r = \sqrt{x^2 + y^2 + z^2} \quad .$$

The components of $\overline{B}_{ms}$ are given in γ. The positive x axis points toward the Sun, the z axis is north, antiparallel to the dipole axis, and the y axis lies in the dusk-meridian plane. Field lines from this expansion and a dipole representation of $\overline{B}_{gm}$ are shown in the noon-midnight meridian on Figure 2-15.

In studies of the inner magnetosphere, where great accuracy in $\overline{B}_{ms}$ is not required, an abbreviated version can be used. A series containing only linear and quadratic terms (including exponential terms) was developed for this purpose. The same fitting routine was used to orthonormalize the input series. The components of $\overline{B}_{ms}$ were found to be

$$B_x = 0.9535z - 0.00507xz + (2.1143z - 5.246xz)\exp(-0.06r^2) \qquad (2\text{-}18a)$$

$$B_y = -[0.01382 + 6.7682\exp(-0.06r^2)]yz \qquad (2\text{-}18b)$$

$$B_z = 8.196 + 1.363x - 0.01524z^2 + 0.0088y^2 + 0.0609x^2 + (-8.803 + 3.578x - 1.7927z^2 - 6.0491y^2 - 6.8595x^2)\exp(-0.06r^2) \quad . \qquad (2\text{-}18c)$$

Table 2-3. Coefficients for the quiet-time ring and tail field B_D.

i	j	k	a	b	c	d	e	f
0	0	0	3.03084E-01	-1.20397E+00	-2.66634E-02	-1.56039E+00	6.89827E+01	-1.61132E+02
0	0	1	9.94259E-04	-5.18429E-04	5.09343E-05	2.62908E-02	-3.18015E-01	-7.49275E-01
0	0	2	-1.65861E-05	-1.59620E-04	-2.63356E-08	-3.00649E-04	3.57573E-04	-5.88638E-03
0	0	3	3.89586E-08	-7.40696E-07			-1.49037E-08	-4.69035E-06
0	1	0	-3.11960E-03	-4.06538E-04	3.16180E-05	-5.11911E-02	-5.16027E-02	-3.79609E+00
0	1	1	1.27319E-05	7.27348E-04	-2.18586E-07	6.22798E-04	3.46543E-04	2.55804E-02
0	1	2	-8.25454E-09	-1.75181E-05			-5.35861E-07	-1.62589E-04
0	2	0	3.97056E-06	-2.45926E-03	-6.66053E-08	-5.63325E-04	1.77600E-04	5.37076E-02
0	2	1	-2.30325E-09	1.53083E-05			-5.16099E-07	-5.94940E-04
0	3	0	1.16469E-08	1.43093E-05			-6.29046E-08	-3.20534E-04
1	0	0	-4.32187E-02	-1.28645E+00	-2.10238E-03	1.24297E-01	8.07648E+00	-1.01167E+01
1	0	1	9.47915E-06	2.57490E-02	1.39874E-06	-3.28318E-03	-2.79426E-02	-7.04255E-02
1	0	2	4.84925E-07	-3.14214E-04	-5.49844E-10	3.14517E-05	1.91885E-05	-4.94555E-04
1	0	3					-5.74976E-10	-1.88974E-06
1	1	0	6.41076E-06	-3.98512E-02	7.89342E-07	-6.71962E-03	2.24550E-03	-3.68784E-02
1	1	1	3.47834E-07	5.31966E-04	-3.59102E-09	5.77080E-05	9.20447E-06	2.69889E-03
1	1	2					-9.03916E-09	-3.58134E-05
1	2	0	2.99772E-07	-4.92982E-04	-1.10645E-09	9.25909E-05	9.20716E-06	2.03563E-04
1	2	1					-8.74839E-09	-6.83030E-05
1	3	0					-1.45008E-09	-2.43156E-05
2	0	0	9.03152E-04	3.25210E-02	-6.23194E-05	-3.06098E-02	4.13834E-01	-3.77235E+00
2	0	1	6.50309E-06	2.16280E-03	3.06589E-09	6.64222E-04	-1.03501E-03	4.41952E-02
2	0	2	6.74264E-09	-3.16332E-05			3.45072E-07	-3.82535E-04
2	1	0	5.06416E-06	-7.58816E-03	-7.68019E-09	-1.73273E-03	3.65050E-04	9.44210E-02
2	1	1	2.71305E-09	-3.33546E-06			5.88306E-08	-1.90770E-03
2	2	0	2.57455E-09	8.67320E-05			1.64155E-07	-1.00580E-03
3	0	0	1.62440E-04	-2.79550E-02	-5.14992E-07	-8.56272E-03	1.16124E-02	3.59912E-03
3	0	1	1.44444E-07	4.53527E-04	-7.76309E-11	6.03088E-05	-1.95219E-05	-6.37663E-04
3	0	2					2.09077E-09	-3.28110E-05
3	1	0	1.04239E-07	-1.46294E-03	-1.10716E-10	1.98384E-04	1.22566E-05	-4.21935E-03
3	1	1					5.75970E-11	-1.09390E-04
3	2	0					1.03832E-09	-2.19306E-05
4	0	0	4.64866E-06	-7.11688E-03	5.08526E-09	-1.05842E-03	1.86319E-04	1.77486E-02
4	0	1	8.04227E-10	-1.04400E-05			-1.84967E-07	-9.89453E-04
4	1	0	6.10089E-10	1.54156E-04			1.65193E-07	-1.00052E-03
5	0	0	5.32811E-08	-8.39786E-04	6.63718E-11	1.22606E-04	1.60729E-06	-2.12577E-03
5	0	1					-7.00807E-10	-3.42765E-05
5	1	0					7.97013E-10	-2.40418E-05
6	0	0	2.21963E-10	8.83005E-05			5.77662E-09	-1.54671E-04

Table 2-4. Coefficients for the boundary field B_{MP}.

i	j	k	a	b	c	d	e	f
0	0	0	4.80089E-01	-1.56051E-01	-6.69399E-02	-8.13476E-02	3.13997E+01	-1.12984E+01
0	0	1	1.86580E-03	7.[illegible]48E-02	1.88237E-05	3.01308E-03	-1.33815E-01	5.33976E-02
0	0	2	-2.93832E-07	-8.49100E-[illegible]	-2.63579E-09	-1.62057E-04	-1.10028E-04	3.05649E-03
0	0	3	-3.27168E-09	3.95509E-05			1.28101E-07	-1.29016E-05
0	1	0	8.33250E-04	4.72493E-02	6.08168E-05	9.52334E-04	-1.30170E-01	-6.04710E-02
0	1	1	-2.67254E-07	-2.33267E-[illegible]	-1.10882E-08	-2.61196E-04	4.99002E-07	-3.43592E-03
0	1	2	-3.50274E-09	5.40872E-05			1.17960E-07	4.34567E-05
0	2	0	-1.72823E-07	-6.29651E-04	1.49477E-09	-3.72611E-05	8.33571E-05	-1.05452E-03
0	2	1	-6.32375E-09	6.74334E-05			3.03366E-07	6.80264E-05
0	3	0	-7.01112E-09	8.33100E-06			1.79113E-07	9.84484E-06
1	0	0	-4.26464E-02	-7.24772E-01	-7.01620E-03	-4.42443E-03	1.99485E+00	-2.81260E-01
1	0	1	2.11234E-04	3.90235E-03	8.03825E-07	5.50251E-04	-1.50609E-02	3.77337E-02
1	0	2	-4.32992E-08	1.63829E-04	-4.21591E-10	5.24365E-08	-5.90082E-06	3.04748E-03
1	0	3					2.41974E-09	3.80169E-08
1	1	0	1.14503E-04	2.25009E-03	4.39372E-06	-9.10022E-05	-1.26121E-02	2.07499E-05
1	1	1	-3.30151E-08	-2.10619E-04	-1.22753E-09	-3.76167E-05	1.73541E-06	1.07613E-03
1	1	2					2.32185E-09	1.32008E-06
1	2	0	-7.88861E-08	1.15465E-04	-9.41669E-10	-5.42501E-06	8.40171E-06	1.21812E-04
1	2	1					6.81964E-09	7.04659E-06
1	3	0					3.98230E-09	7.73475E-07
2	0	0	-6.97385E-03	5.09930E-01	-3.15721E-04	-3.71128E-03	-1.14513E-03	-2.22084E-01
2	0	1	7.70144E-06	-3.92225E-04	6.69570E-09	-4.00593E-05	-6.82897E-04	-8.00477E-03
2	0	2	-2.81406E-10	-3.21207E-05			-1.17705E-07	6.09960E-04
2	1	0	4.56974E-06	-3.68798E-04	1.02190E-07	-1.36987E-05	-4.70111E-04	-3.46000E-03
2	1	1	-8.20743E-11	-9.88631E-05			4.17787E-08	2.78768E-04
2	2	0	-5.96721E-10	3.44622E-05			2.09074E-07	3.20741E-05
3	0	0	-3.30700E-04	7.32979E-03	-7.34171E-06	-2.15299E-04	-3.17143E-03	-1.50116E-02
3	0	1	1.17675E-07	-3.85741E-04	2.94792E-11	-3.10973E-05	-1.53290E-05	-2.36182E-03
3	0	2					-8.52528E-10	3.27262E-05
3	1	0	7.67127E-08	8.97337E-05	8.54549E-10	1.09508E-05	-8.62171E-06	-2.21193E-04
3	1	1					1.38172E-10	1.91697E-05
3	2	0					1.41658E-09	2.36438E-06
4	0	0	-7.48780E-06	-1.74685E-02	-8.57248E-08	1.01171E-04	-1.01101E-04	-5.88840E-06
4	0	1	6.41093E-10	3.97861E-05			-1.68810E-07	-1.77100E-04
4	1	0	4.56256E-10	5.62987E-05			-7.95873E-08	2.59990E-05
5	0	0	-8.29848E-08	4.51102E-04	-3.97267E-10	1.10160E-05	-1.27463E-06	6.97685E-05
5	0	1					-7.25781E-10	-1.70500E-06
5	1	0					-2.98796E-10	3.15401E-06
6	0	0	-3.60710E-10	1.35731E-04			-5.85771E-09	-3.78849E-06

Table 2-5. Coefficients for the total external field $B_{MP} + B_D$.

i	j	k	a	b	c	d	e	f
0	0	0	7.83174E-01	-1.36002E+00	-9.36032E-02	-1.64174E+00	1.00382E+02	-1.12431E+02
0	0	1	2.88006E-03	7.80264E-02	6.97561E-05	2.93038E-02	-9.51830E-01	-6.95878E-01
0	0	2	-1.68900E-05	-1.00872E-03	-2.89714E-08	-4.62707E-04	2.47545E-04	-2.82989E-03
0	0	3	3.55369E-08	3.88102E-05			1.13197E-07	-1.75919E-05
0	1	0	-2.28540E-03	4.68426E-02	1.12435E-04	-5.02388E-02	-1.81773E-01	-3.85656E+00
0	1	1	1.24647E-05	4.94081E-04	-2.29674E-07	3.61602E-04	3.47042E-04	2.21445E-02
0	1	2	-1.17573E-08	3.65692E-05			-4.17901E-07	-1.19133E-04
0	2	0	3.79774E-06	-3.08892E-03	-6.51105E-08	-6.00587E-04	2.60957E-04	5.26531E-02
0	2	1	-8.62700E-09	8.27418E-05			-2.12733E-07	-5.26914E-04
0	3	0	4.63581E-09	2.26403E-05			1.16209E-07	-3.10689E-04
1	0	0	-8.58651E-02	-2.01122E+00	-9.11858E-03	1.19872E-01	1.00710E+01	-1.03980E+01
1	0	1	2.20713E-04	2.96513E-02	2.20257E-06	-2.73293E-03	-4.30035E-02	-3.26917E-02
1	0	2	4.41626E-07	-1.50385E-04	-9.71435E-10	3.15041E-05	1.32877E-05	2.55292E-03
1	0	3					1.84477E-09	-1.85172E-06
1	1	0	1.20914E-04	-3.76012E-02	5.18306E-06	-6.81062E-03	-1.03666E-02	-3.68576E-02
1	1	1	3.14819E-07	3.21347E-04	-4.81855E-09	2.00913E-05	1.09399E-05	3.77502E-03
1	1	2					-6.71731E-09	-3.44933E-05
1	2	0	2.20886E-07	-3.77516E-04	-2.04812E-09	8.71659E-05	1.76089E-05	3.25375E-04
1	2	1					-1.92875E-09	-6.12564E-05
1	3	0					2.53223E-09	-2.35422E-05
2	0	0	-6.07070E-03	5.42451E-01	-3.78041E-04	-3.43211E-02	4.12689E-01	-3.99444E+00
2	0	1	1.42045E-05	1.77058E-03	9.76159E-09	6.24163E-04	-1.71790E-03	3.61904E-02
2	0	2	6.46123E-09	-6.37539E-05			2.27366E-07	2.27425E-04
2	1	0	9.63390E-06	-7.95695E-03	9.45094E-08	-1.74643E-03	-1.05062E-04	9.09610E-02
2	1	1	2.63098E-09	-1.02199E-04			1.00609E-07	-1.62893E-03
2	2	0	1.97783E-09	1.21194E-04			3.73228E-07	-9.73721E-04
3	0	0	-1.68259E-04	-2.56253E-02	-7.85671E-06	-8.77802E-03	8.44098E-03	-1.14125E-02
3	0	1	2.62119E-07	6.77865E-05	-4.81517E-11	2.92115E-05	-3.48509E-05	-2.99948E-03
3	0	2					1.23824E-09	-8.48886E-08
3	1	0	1.80952E-07	-1.37321E-03	7.43833E-10	2.09335E-04	3.63487E-06	-4.44055E-03
3	1	1					1.95769E-10	-9.02203E-05
3	2	0					2.45490E-09	-1.95662E-05
4	0	0	-2.83914E-06	-2.45654E-02	-8.06396E-08	-9.57252E-04	8.52182E-05	1.77427E-02
4	0	1	1.44532E-09	2.93461E-05			-3.53777E-07	-1.16655E-03
4	1	0	1.06634E-09	2.10455E-04			8.56056E-08	-9.74518E-04
5	0	0	-2.97037E-08	-3.88684E-04	-3.28896E-10	1.33622E-04	3.32657E-07	-2.05600E-03
5	0	1					-1.42659E-09	-3.59815E-05
5	1	0					4.98217E-10	-2.08878E-05
6	0	0	-1.38747E-10	2.24031E-04			-8.10951E-11	-1.58459E-04

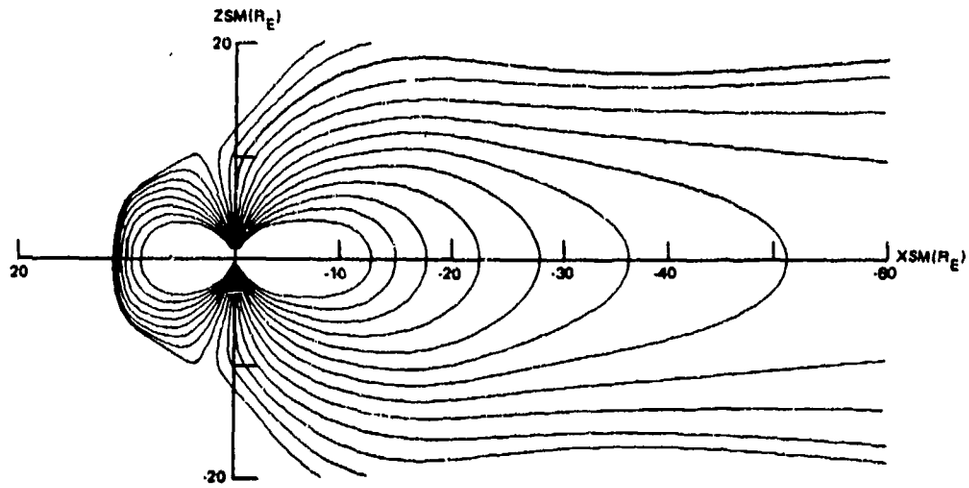

Figure 2-15. Magnetic field lines in 2-degree intervals from 70 degrees latitude to pole in noon-midnight meridian plane.

The components of $\overline{B}_{ms}$ are analytic and differentiable, as they are in the sixth-order expansion. The inclusion of the exponential terms makes it possible to model the near-Earth field depressions, ΔB, produced by the quiet-time ring current. These simple expressions yield ΔB contours that exhibit the basic features found in the observational data.

The z component of the magnetospheric magnetic field (minus the main field of the Earth) is shown along the Earth-Sun line on Figure 2-16. (By symmetry, the field is in the z direction along this line.) The observed field exhibits considerable structure within a geocentric distance of 5 R_E because of the disturbed magnetospheric currents. The difference between the present sixth-order models and the older models that included only the boundary (magnetopause) currents is as large as 65 γ, and near 6 R_E it is about 40 γ (approximately 35 percent of the total field). Similar large differences in the total field are found throughout the inner magnetosphere. It is, therefore, expected that there would be appreciable differences between this model and previous ones when they are used to calculate magnetospheric particle and field properties.

2.5.3 Comparisons of Olson-Pfitzer Models with Observed Particle and Field Behavior

Optical tracking data from the NASA-MPE barium cloud experiment have shown that field lines in the inner magnetosphere are more

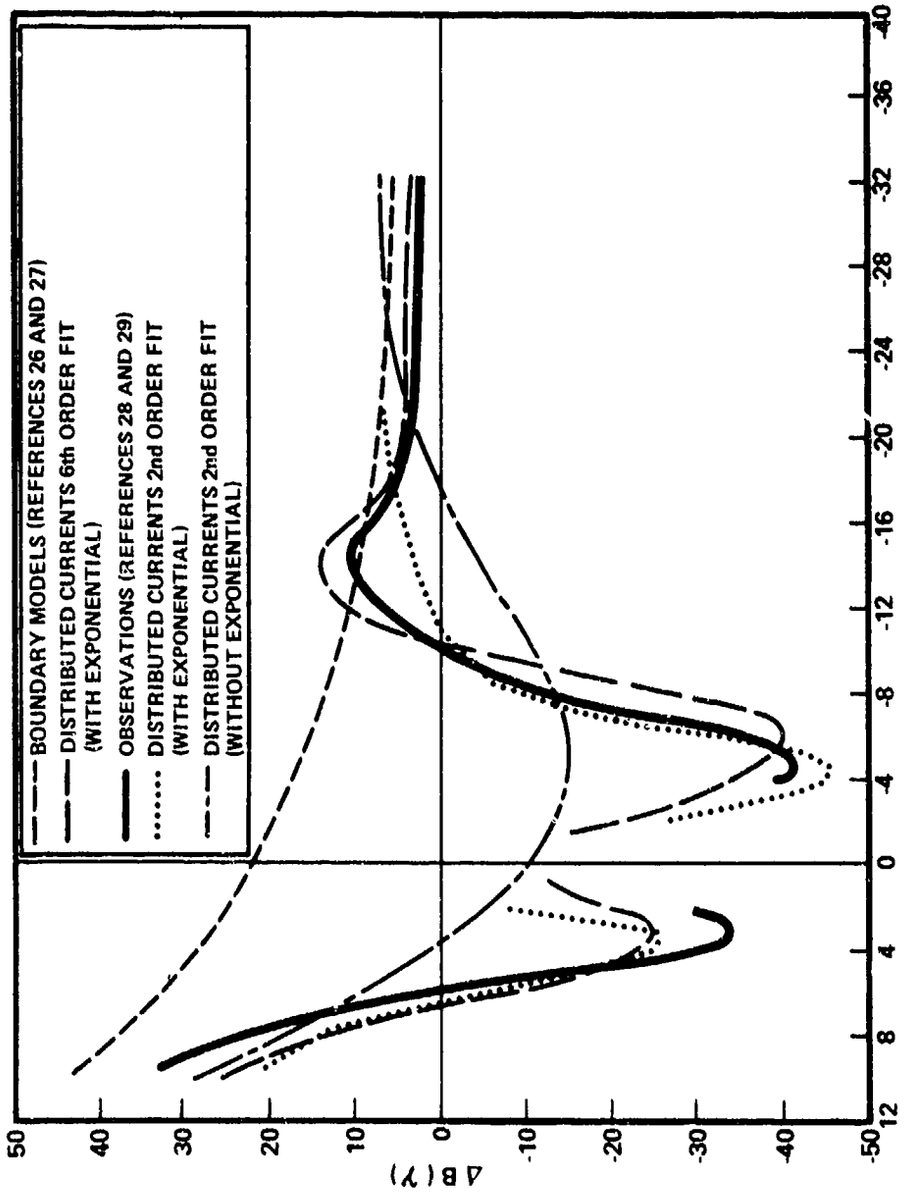

Figure 2-16. The z component of the magnetospheric field (minus the Earth's main field) along the Earth-Sun line.

elongated than the lines calculated from models consisting of main field and earlier external field representations. Olson-Pfitzer models fit the observations quite accurately (Figure 2-17) because they include the depressed inner magnetosphere field features produced by the quiet-time ring current. Field lines calculated from other models that do not include this feature are inclined by as much as 15 degrees to the field line along the barium cloud.

The Earth intercepts of field lines from geosynchronous orbit (6.6 R_E) have been determined for various local times (Figure 2-18). Both second-order and sixth-order expansions place the latitude of the foot of the line at about 65 to 66 degrees, depending upon the time of day, which is about 4 degrees lower than that predicted by the "boundary only models." This difference too is believed to result from the quiet-time ring currents that produce the depressed field region near the Earth. Both the second-order and sixth-order models indicate that the field lines to geosynchronous orbit are more extended than dipolar field lines.

The sixth-order model has been used to compute low- and high-energy charged particle behavior in the magnetosphere. The high-latitude Earth intercept of the trapping boundary calculated from the model agrees well with the observed boundary, which is 4 to 5 degrees lower than that calculated from previous models. The boundary was found by using the first- and second-adiabatic invariants to calculate the last closed drift shell on which a particle with a given pitch angle can exist.

The high-latitude cutoffs for cosmic-ray particles calculated from previous models have been in error with observation by 5 to 7 degrees. With the present models, the calculated cutoffs are essentially in agreement with the observed values (Reference 33). The cutoffs have been determined for 5, 20, and 70 MeV by utilizing the distributed current model. Again, it is the depressed field region for 3- to 6-R_E geocentric distance produced by the distributed currents that causes the field lines at a given latitude on the Earth's surface to cross the equator at larger geocentric distances than those calculated from previous models. In turn, it is this field geometry that allows charged particles to penetrate to lower latitudes than is possible with models that do not include the effects of distributed currents that flow through the inner magnetosphere.

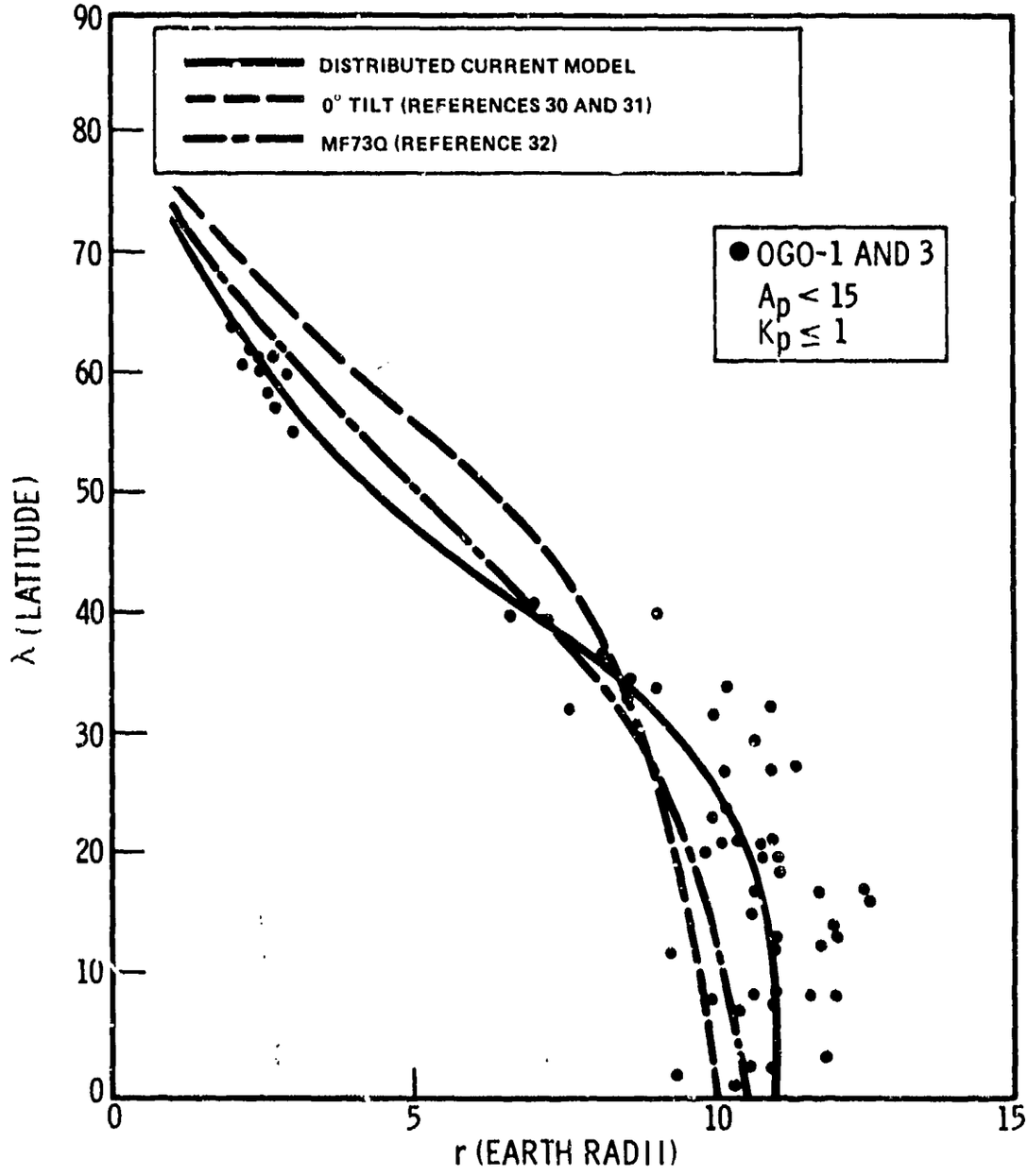

Figure 2-17. Comparison of theoretical and experimental spatial coordinates along field lines.

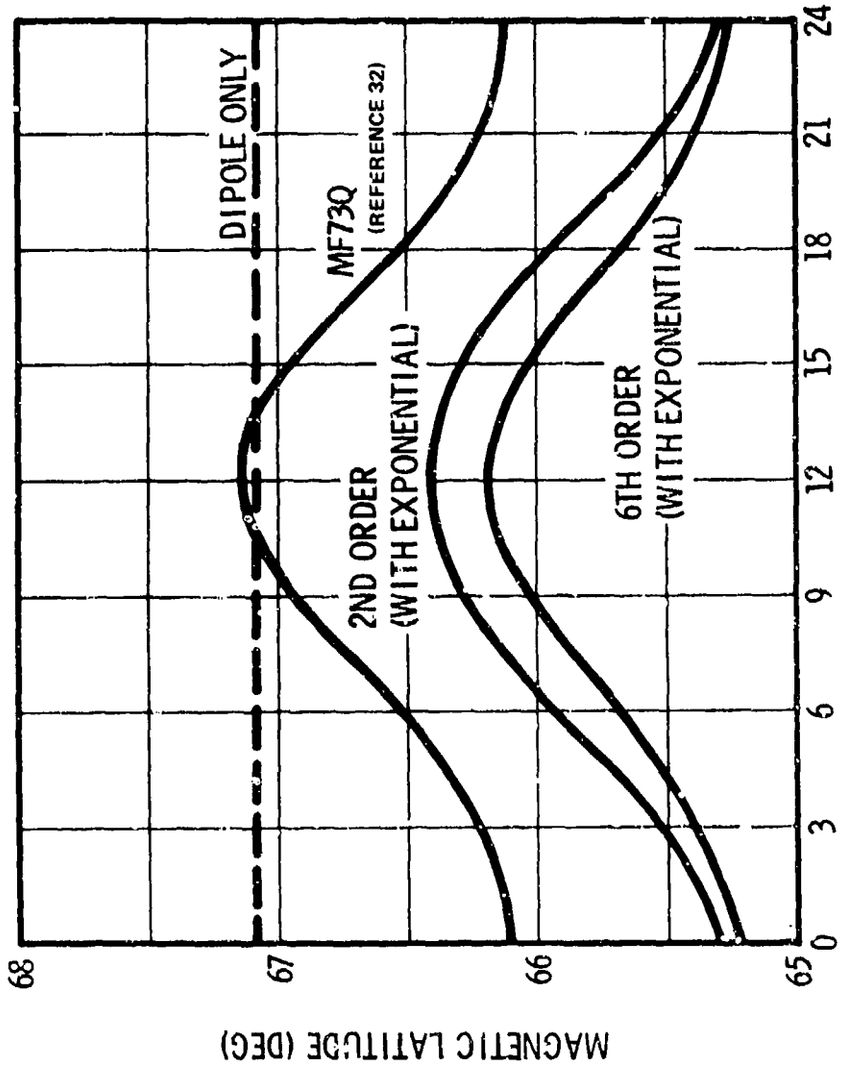

Figure 2-15. Latitude of geosynchronous field line at Earth intercept.

2.6 GEOMAGNETIC TRANSIENT VARIATIONS

2.6.1 Solar Quiet and Lunar Daily Variations

The continuous traces of the three magnetic elements recorded at any station consistently show a daily time variation that is correlated with local time. The maximum variation occurs near local noon and is on the order of 0.1 percent of the total field. On some days, the variations are smooth and regular; on other days, the changes are irregular because of magnetic disturbances superimposed on the smooth variation. The days in which irregular variations are recorded are said to be magnetically active or disturbed days; those with smooth traces are called magnetically quiet days.

The average variation patterns, derived for the field components from suitably chosen quiet-day records at a station, collectively define a variation field denoted by Sq, the solar quiet daily variation. For each component, the variation is reckoned using the daily mean value of the component at the station as a base line. The global distribution of Sq varies systematically with latitude. In the magnetic equatorial zone, the maximum variation in the horizontal intensity H near local noon is characteristically about 100 gammas, and at higher latitudes it is -25 to -50 gammas.

Sq is also dependent on the season of the year and the phase of the solar cycle. At the June solstice, Sq is enhanced in the northern hemisphere and diminished in the southern hemisphere. At the December solstice, the situation is reversed. At sunspot maximum, Sq increases.

The daily variation of the field also includes a component having a period of 0.5 lunar day ($\approx$ 12.42 hours) and a pattern that varies systematically with the phase of the Moon. This variation is less than 0.1 that of Sq. The average of this component of the magnetic variation over many lunar days at a station is called the lunar daily variation, L, (not to be confused with the L shell parameter). L is somewhat enhanced during sunlight hours and displays seasonal changes indicating that the Sun, as well as the Moon, plays a controlling role.

Spherical harmonic analysis of Sq or L data from a world network of stations is used to determine the equivalent electric current systems responsible for the observed magnetic variations. About two-thirds of the variations in Sq or in L is found to be due to current sources external to the Earth and the remaining one-third to

internal currents induced within the Earth's surface layers by variable external currents. The external currents responsible for Sq and L are found to flow at approximately the same altitude (~100 kilometers). The ratio of average external Sq and L current intensities is about 30 to 1.

The Sq and L electric current systems are produced by convective movement of the conducting upper atmosphere across the Earth's magnetic field lines. The motion of the upper atmosphere occurs as a result of pressure and temperature differentials in the atmosphere brought about by solar heating and tidal forces. By analogy with an electric dynamo, this mechanism is referred to as the atmospheric dynamo (Reference 34).

For a detailed discussion of solar quiet and lunar daily variations, including plots of Sq and L and their associated current systems, see Reference 35.

From rocket measurements, X-rays are known to be emitted by solar flares. On arrival at Earth, these X-rays cause an increase in ionization in the sunlit hemisphere, particularly at lower levels. The overhead current system is enhanced, often producing an observable magnetic field variation called a solar flare effect (sfe) or a crochet (Reference 36). The variation lasts 10 to 60 minutes and is manifested as an augmentation of Sq. Ionospheric currents due to solar flares occur lower in the ionosphere than Sq currents and sometimes seem to flow in the night hemisphere but with reduced intensity.

2.6.2 Geomagnetic Storms

A severe and long-lasting magnetic disturbance that occurs worldwide is called a magnetic storm (References 36 and 37) and often is accompanied by auroral displays and polar ionospheric disturbances. The rate of occurrence of magnetic storms varies with the solar sunspot cycle.

Magnetograms obtained at low- and middle-latitude stations indicate that many storms undergo a similar pattern of development as the storms progress. The start of a typical storm is characterized by an abrupt increase in H and is known as the sudden commencement (S.C.) of the storm. The increase is typically 20 to 30 gammas with a rise time of 2 to 6 minutes; it is largest at stations near the magnetic equator. The 2- to 8-hour interval during which the value

of H remains above its undisturbed value is known as the initial phase of the storm.

The main phase of the storm follows and lasts 12 to 24 hours during which H decreases to values that are typically 50 to 100 gammas below the prestorm value. The final stage of the storm, known as the recovery phase, commences and H gradually recovers to its normal level in 1 to 3 days, although recovery time as long as 20 to 30 days is not uncommon. Individual storm records show irregularities. The initial and main phases tend to be noisy. Often during the main phase, large amplitude fluctuations occur with periods of about 0.5 hour. Some storms do not conform to this classic pattern and have features that are missing or not easily identified.

The simultaneous storm records obtained at auroral zone and polar cap stations are markedly different from this regular storm pattern and are characterized by extremely large and sometimes very rapid changes. Careful analysis is required to detect the regular storm variations in the high-latitude records.

The analysis of storms has shown that the typical storm variation over the Earth can be described conveniently by two components: (1) Dst (or DST), which is symmetric about the geomagnetic axis; and (2) DS (or Ds), which is a function of longitude relative to the Sun (Reference 36). Both components are also dependent on magnetic latitude and storm time (time measured from the start of the storm).

Changes in the dynamic pressure of the solar wind blowing against the geomagnetic field are believed to be a cause of magnetic storms (Reference 38). The solar wind suddenly increases, compressing the magnetic field (S.C.) and maintains the compression for a time (initial phase). An outward distention then occurs (main phase) and is followed by a relaxation of the field to its prestorm value (recovery phase). Some uncertainty exists whether the main phase is produced by an outward distention of the field because of hot plasma generated by attendant processes or whether, instead, the main phase is produced by a westward ring current (circling the Earth at several Earth radii) consisting of electrons and positive ions that are trapped or injected in the magnetosphere (Reference 36).

Recent experiments suggest that an increase in solar wind pressure may not be a necessary condition for the generation of all magnetic

storms (References 39 and 40). Instead, the southward component of the interplanetary field appears to play the major role, an enhancement in this component being strongly correlated with the initiation of some magnetic storms.

2.6.3 Sudden Impulses and Bays

An impulsive change (generally an increase of several gammas in the magnetic field followed by a gradual return to the normal field value and without subsequent large field changes is called a sudden impulse (S.I. or si) (Reference 36). The changes occur simultaneously at stations all over the world and are similar in characteristics to S.C.s, but have smaller amplitudes and less abrupt changes in field intensity.

Another type of simple magnetic disturbance is characterized by a gradual increase or decrease in the field followed by a return, perhaps with small oscillations, to the undisturbed field value. These disturbances last 1 to 2 hours and generally are preceded and followed by undisturbed conditions. The horizontal component of the field is affected most strongly and departs from undisturbed field values by 5 to 20 gammas at midlatitude stations and is perhaps a factor of 10 greater at higher latitudes. These disturbances are known as magnetic bays because the resulting curves of field intensity (principally H) recorded at a station resemble a bay as it appears drawn on a map (Reference 41). Magnetic bays are most pronounced at high latitudes and occur principally at night near local midnight. Positive bays occur several times more frequently than to negative bays. The generation of magnetic bays and sudden impulses is related to changes in the solar wind pressure and to changes in the southward component of the interplanetary field (References 39 and 40).

2.7 GEOMAGNETIC PULSATIONS

2.7.1 Micropulsations

Micropulsations are geomagnetic field fluctuations that occur in the ultra-low frequency (ULF) region below about 3 Hertz (Reference 42). They have periods ranging from about 0.2 second to 10 minutes and amplitudes varying from a fraction of one gamma to several tens of gammas. Figure 2-19 is an approximate representation of the power spectrum of magnetic fluctuations at the Earth's surface (References 42, 43, and 44). The figure is a composite of data recorded

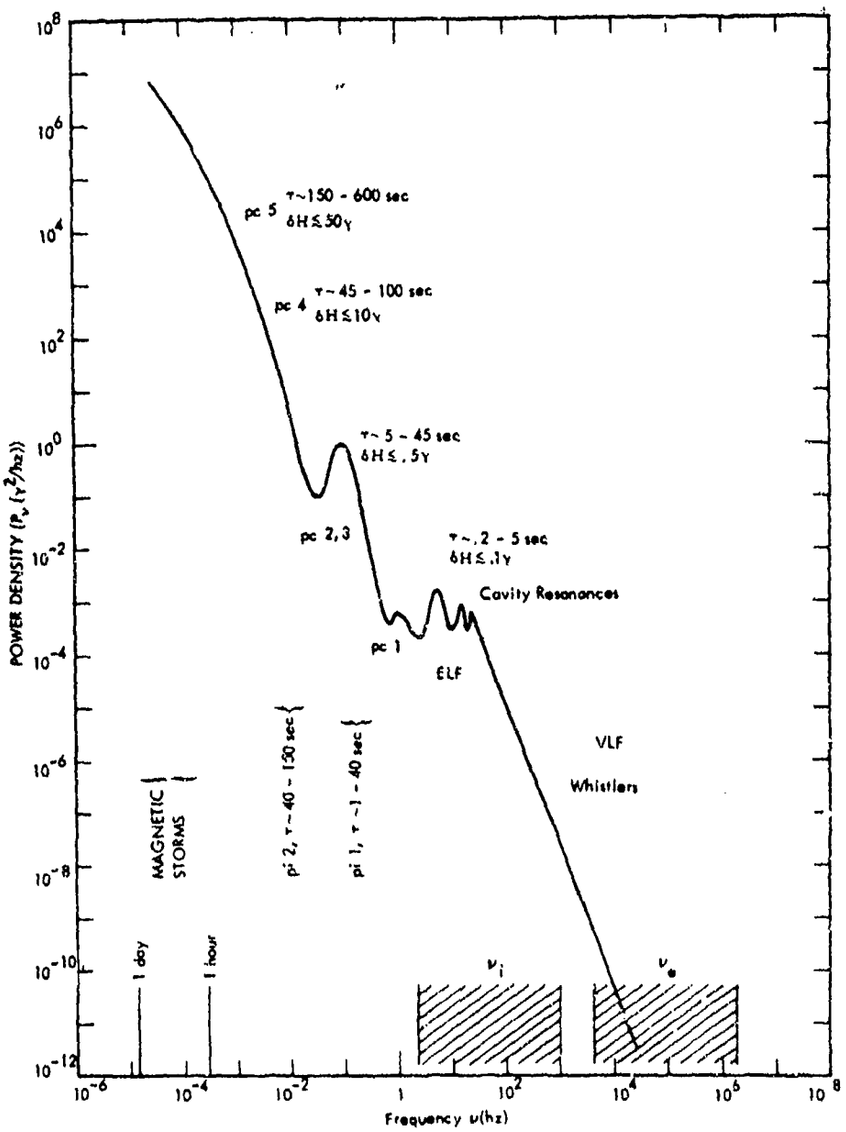

Figure 2-19. Power spectrum of geomagnetic disturbances observed on the Earth's surface.

in various frequency ranges (References 43 and 45 through 49). Although the general trend of the data presented on the figure may be accepted as a fair representation of actual average conditions, substantial uncertainties still exist in the interrelationship between various types of disturbances. The ranges of proton and electron gyrofrequencies, ν_i and ν_e, respectively, are indicated. The range of periods τ and characteristic amplitudes δH are indicated for several classes of fluctuations. The micropulsation spectrum is bordered at low frequencies by storm time and Sq phenomena and at high frequencies by extra-low frequency (ELF) phenomena.

Certain types of micropulsations have been classified according to the assignments shown on Figure 2-19. Micropulsations are divided into two general types: continuous pc, and irregular pi. A pc micropulsation displays amplitude variations that are quasi-sinusoidal. A pi micropulsation has irregularities in both frequency and amplitude. The pc-1 pulsations have amplitude traces that resemble beads on a string and are sometimes referred to as pearls (also hydromagnetic, hm, emissions, and pp). In older literature, pc 5s were known as giant pulsations (Pg) because of large amplitudes.

2.7.2 ELF Pulsations

Pulsation frequencies ranging from about 3 to 3,000 Hertz make up the ELF region. The principal pulsations occurring in this frequency range are ELF sferics slow-tails, Earth-ionosphere cavity resonances, and ELF emissions (Reference 42).

Sferics (an abbreviation for atmospherics) are electromagnetic signals from atmospheric electrical discharges that propagate in the wave guide formed by the ground and the lower edge of the ionospheric E-region (Reference 50). The waveform of a sferic recorded at a large distance from the source consists of a main high-frequency (mostly VLF) oscillatory head, frequently followed by a lower frequency (ELF) tail-like oscillation that is sometimes referred to as a slow-tail (Reference 51). Slow-tails commonly last about 20 milliseconds and have frequency components mainly in the range 30 to several hundred Hertz.

Cavity resonance signals are disturbances that are resonantly excited by lightning transients in the concentric spherical cavity formed by the Earth's surface and the lower region of the ionosphere (Reference 52). The power spectra of the signals often show maxima near 7.8, 14.1, 20.3, 26.4, and 32.5 Hertz.

Occasionally, whistlers and other phenomena that normally occur at higher frequencies in the VLF (very low frequency) range sometimes produce lower frequency components in the ELF region. Also, proton whistlers (Reference 53) and emissions (Reference 54), attributed to radiation at the gyrofrequency of auroral protons, have been observed in the ELF range.

2.7.3 Whistlers and VLF Emissions

Whistlers are field pulsations observed in the frequency range from 300 to 30,000 Hertz (Reference 55). They are produced by the electromagnetic disturbance from lightning. A part of the energy from the disturbance penetrates the ionosphere and propagates along geomagnetic field lines to the opposite hemisphere. The higher frequency components of the disturbance signal arrive first as a result of wave dispersion by the ionosphere. Much of the power is in the audio range (50 to 20,000 Hertz). After conversion to audible sound, the signal is perceived as a variable pitch "whistle" lasting a fraction of a second to 2 or 3 seconds. Whistler echoes often are produced when the signal is reflected several times from the end points of its path. Whistlers are more apt to occur at nighttime, probably because of reduced absorption in the ionosphere. The peak in whistler activity occurs near 50-degree geomagnetic latitude; few whistlers are heard near the geomagnetic equator or poles. Nuclear detonations also produce whistlers with characteristics essentially the same as those of natural whistlers.

VLF emissions are other phenomena having frequencies in the whistler range (Reference 55) and are believed to originate from the excitation of whistler mode waves by charged particles streaming along field lines. The most common VLF emission is known as chorus (or dawn chorus) and consists of a series of oscillations producing sounds that resemble birds chirping at dawn. Another kind of emission is a noise known as hiss, produced by continuous broadband emission in the 1- to 20,000-Hertz range. Periodic VLF emissions are a type consisting of short bursts repeated at regular intervals, typically of several seconds. They are believed to be caused by a whistler and its echoes triggering other emissions in the ionosphere, perhaps through the agency of streaming instabilities (Section 5). A complete discussion of these and other types of VLF emissions is contained in Reference 55.

THIS PAGE IS INTENTIONALLY LEFT BLANK.

APPENDIX 2A
GEOMAGNETIC INDICES

The K-index is designed to measure the degree of magnetic disturbance produced at a station by the solar wind, geomagnetic field interaction. It is intended to serve as an indicator of solar wind activity and is determined at a station for every 3-hour interval during the day, commencing at 0000 Universal Time.

K is based on the amplitude range R of the most disturbed magnetic component observed within a 3-hour interval at the station after Sq and L variations, solar flare effects, and long-term recovery effects have been eliminated from the observations. The ranges of R (in gammas) that define K on a quasi-logarithmic scale for the standard (midlatitude) magnetic observatory are shown in Table 2A-1.

Table 2A-1. Ranges of R (in gammas) that define K on a quasi-logarithmic scale.

K	R (γ)	K	R (γ)
0	0 - 5	5	70 - 120
1	5 - 10	6	120 - 200
2	10 - 20	7	200 - 330
3	20 - 40	8	330 - 500
4	40 - 70	9	≥ 500

To take the latitude dependence of magnetic variations into account, different R scales are adopted at other stations to yield frequency distributions in K that agree with the distribution at the standard observatory. Thus, a K of 9 represents 300 gammas or more at low latitudes and 2,500 gammas or more at auroral zone stations.

The Kp (planetary) 3-hour index is designed to measure the worldwide, or planetary, geomagnetic activity and is based on K-values from

12 stations located at magnetic latitudes varying from 48 to 63 degrees. These K-indices are processed to eliminate local effects and then translated into standardized indices Ks on a finer scale of 28 grades from 0o, 0+, 1-, 1o, 1+, 2-, 2o, 2+, 3-, ... to 7+, 8-, 8o, 8+, 9-, 9o. Kp is the average of the 12 Ks values and also is expressed on the same scale as Ks. A Kp value of 0o indicates an exceptionally quiet period and the value 9o denotes the most severe storm conditions.

A measure of magnetic activity that is approximately linear is sometimes preferred for certain investigations. The 3-hour equivalent planetary amplitude, called ap, was constructed for this purpose by converting Kp to the scale shown in Table 2A-2.

Table 2A-2. Equivalent amplitude ap versus Kp.

Kp	ap	Kp	ap
0o	0	5-	39
0+	2	5o	48
1-	3	5+	56
1o	4	6-	67
1+	5	6o	80
2-	6	6+	94
2o	7	7-	111
2+	9	7o	132
3-	12	7+	154
3o	15	8-	179
3+	18	8o	207
4-	22	8+	236
4o	27	9-	300
4+	32	9o	400

The numerical value of ap is said to be in units of 2 gammas (e.g., for Kp = 4+, ap = 64 gammas) because at the standard observatory the average range in gammas of the most disturbed field element for a given Kp is twice ap. When the eight ap values for one day are

averaged, a new index Ap is obtained known as the daily equivalent planetary amplitude.

Similar scales also have been derived for individual stations and are termed ak and Ak. The index ak, known as the equivalent 3-hour range, is a reconversion of K into a linear scale, and the index Ak, called the equivalent daily amplitude at a station, is the average of the eight ak values for a day. A detailed discussion of magnetic indices is given in Reference 56.

THIS PAGE IS INTENTIONALLY LEFT BLANK.

APPENDIX 2B

MAPS OF THE GEOMAGNETIC LATITUDE AND LONGITUDE

This appendix contains north polar, south polar, and world maps of geomagnetic latitude and geomagnetic longitude at the Earth's surface and at 3,000-kilometers altitude (Reference 9). The plots are based on the IGRF field model (References 7 and 8) for epoch 1969.75. λ and ϕ are geographic latitude and longitude, and Λ and Φ are geomagnetic latitude and longitude.

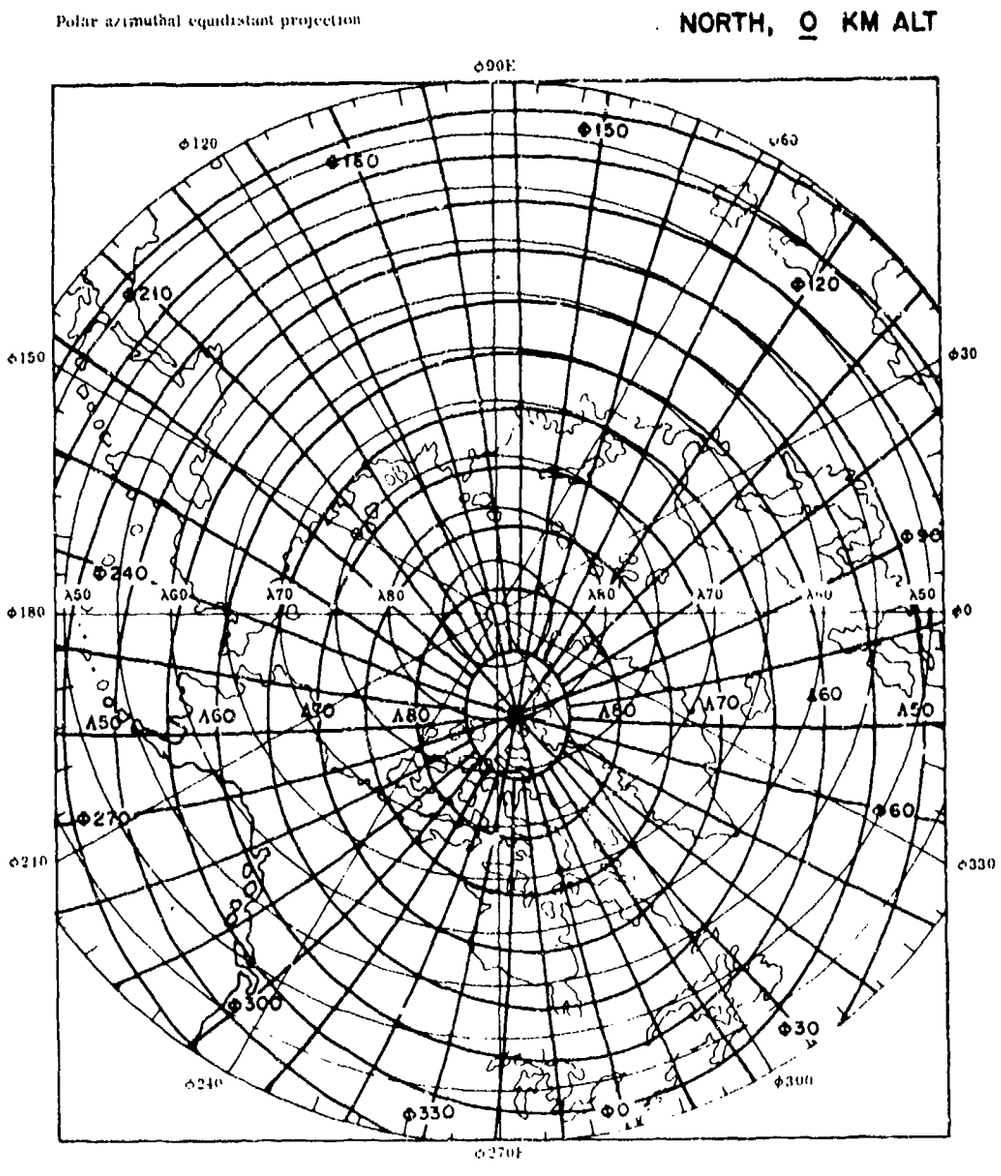

Figure 28-1. North polar plot of geomagnetic coordinates at 0-kilometer altitude.

Polar azimuthal equidistant projection

SOUTH, 0 KM ALT

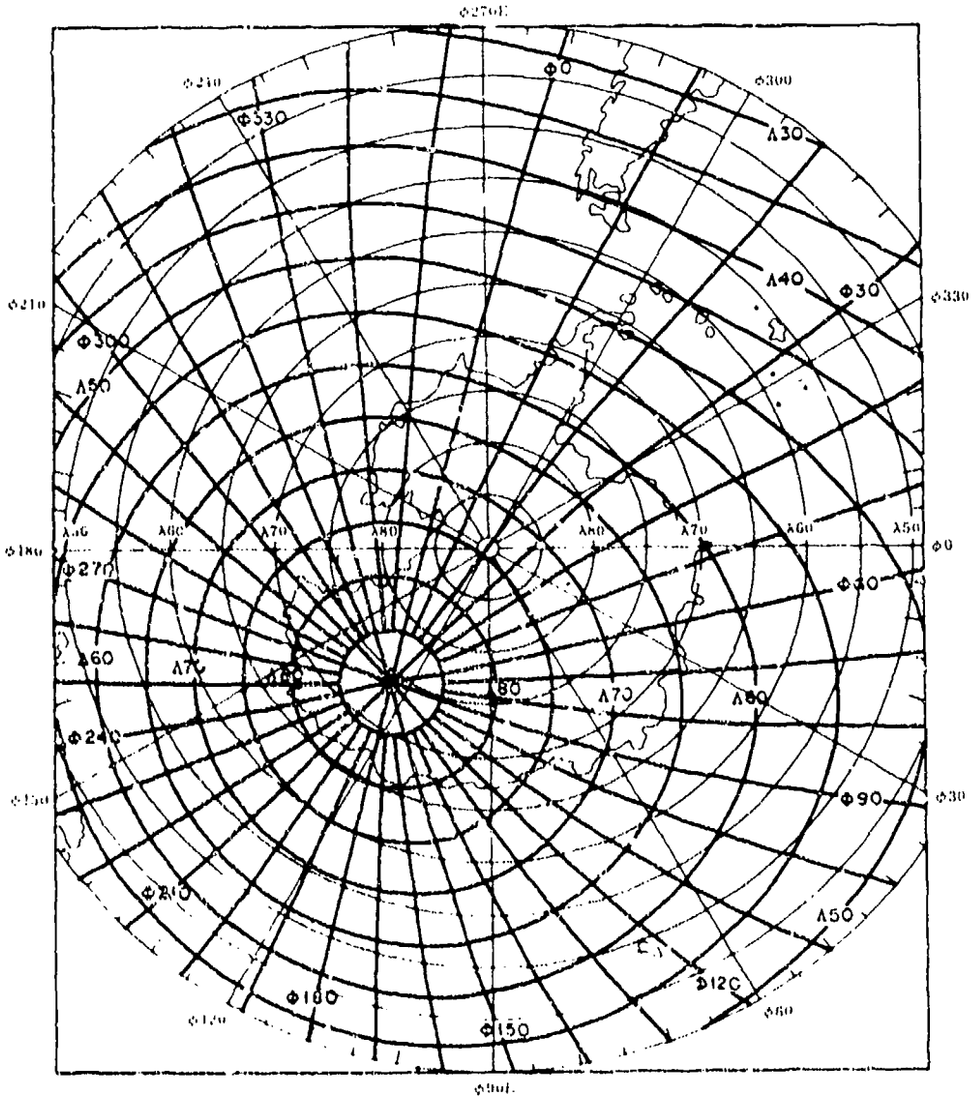

Figure 2B-2. South polar plot of geomagnetic coordinates at 0-kilometer altitude.

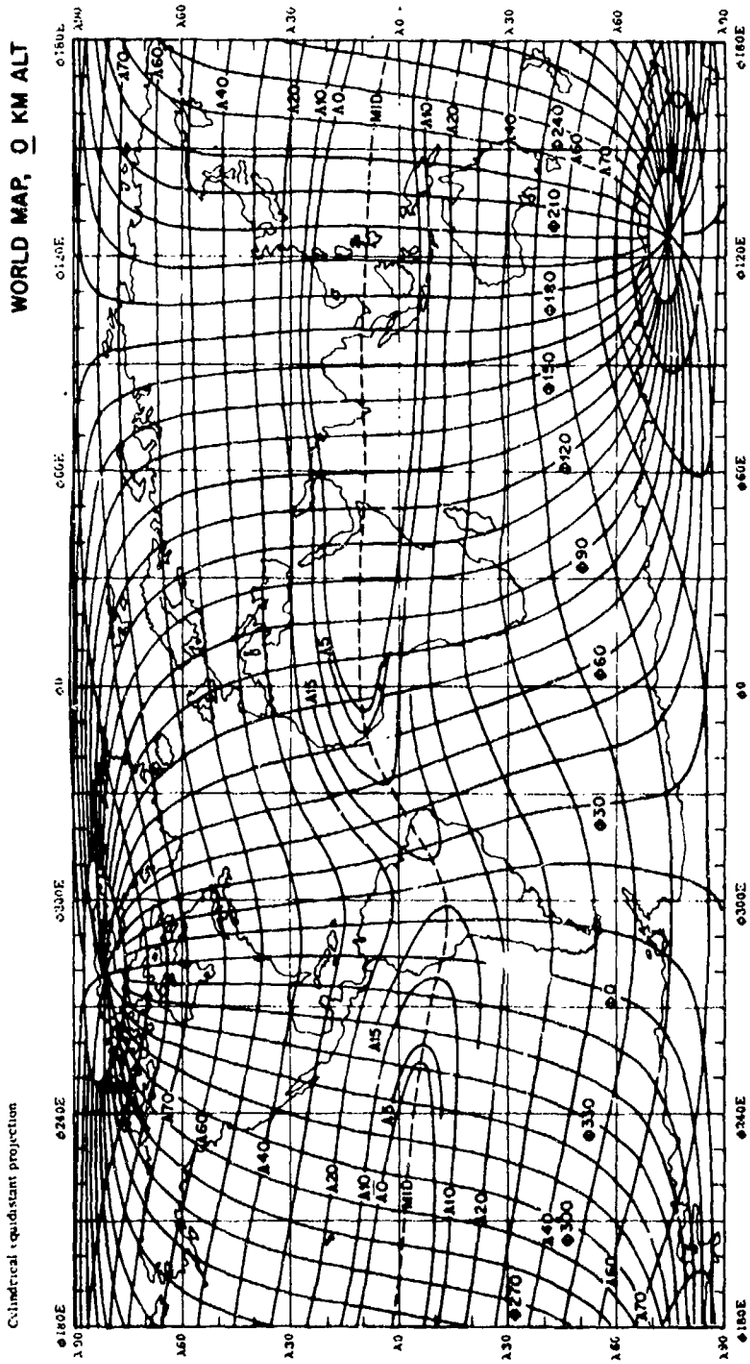

Figure 2B-3. World map of geomagnetic coordinates at 0-kilometer altitude.

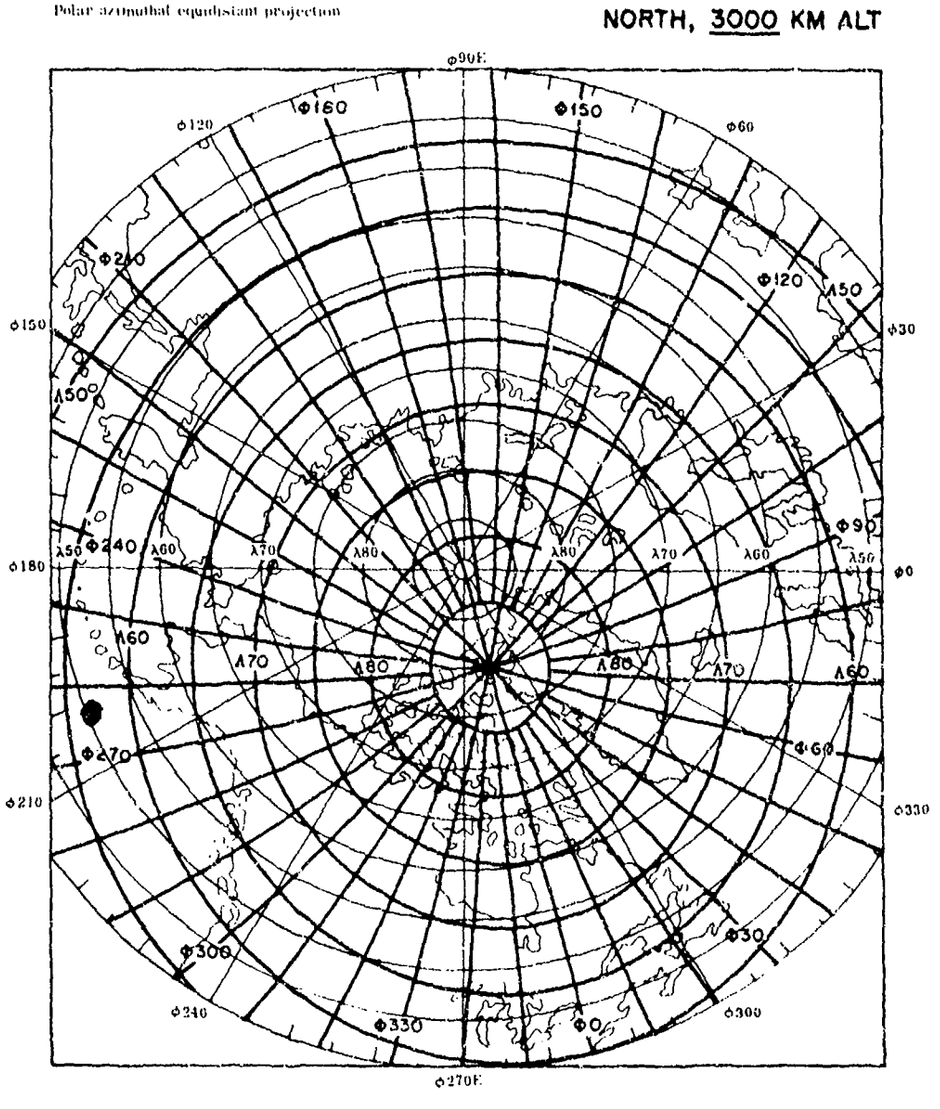

Figure 28-4. North polar plot of geomagnetic coordinates at 3,000-kilometer altitude.

Polar azimuthal equidistant projection

SOUTH, 3000 KM ALT

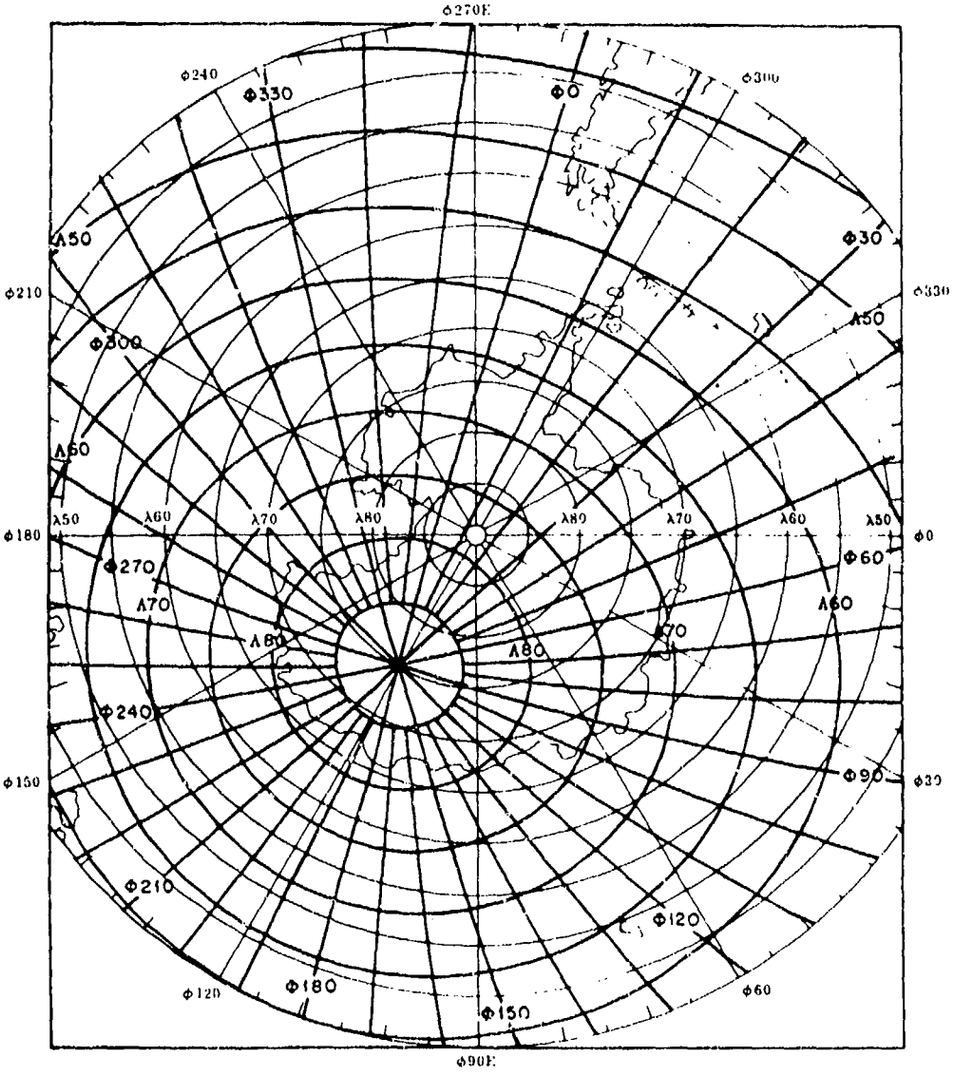

Figure 2B-5. South polar plot of geomagnetic coordinates at 3,000-kilometer altitude.

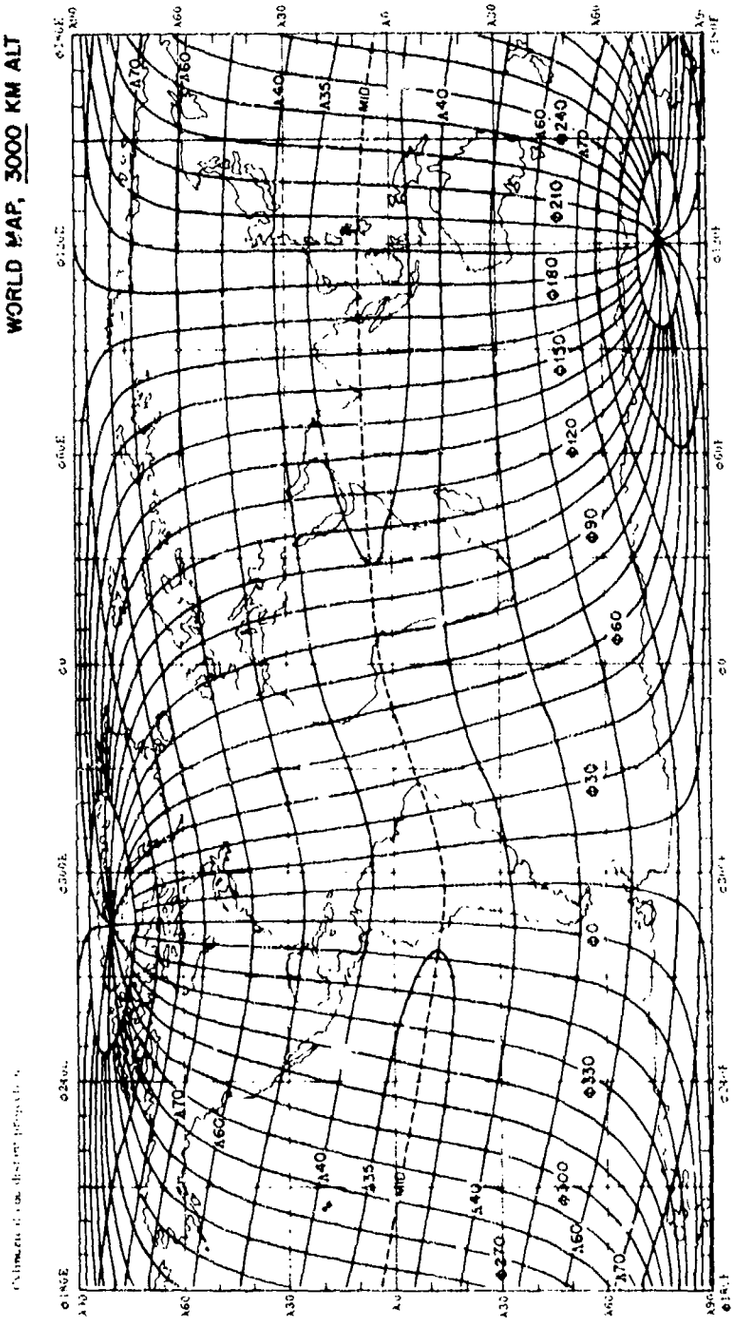

Figure 28-6. World map of geomagnetic coordinates at 3,000-kilometer altitude.

THIS PAGE IS INTENTIONALLY LEFT BLANK.

21 January 1977

APPENDIX 2C
CONTOURS B, L FOR VARYING ALTITUDES

This appendix contains contours of constant-B in gauss and contours of constant-L in Earth radii at 100-, 400-, 800-, 1,600-, and 2,000-kilometer altitudes (References 14 and 57).

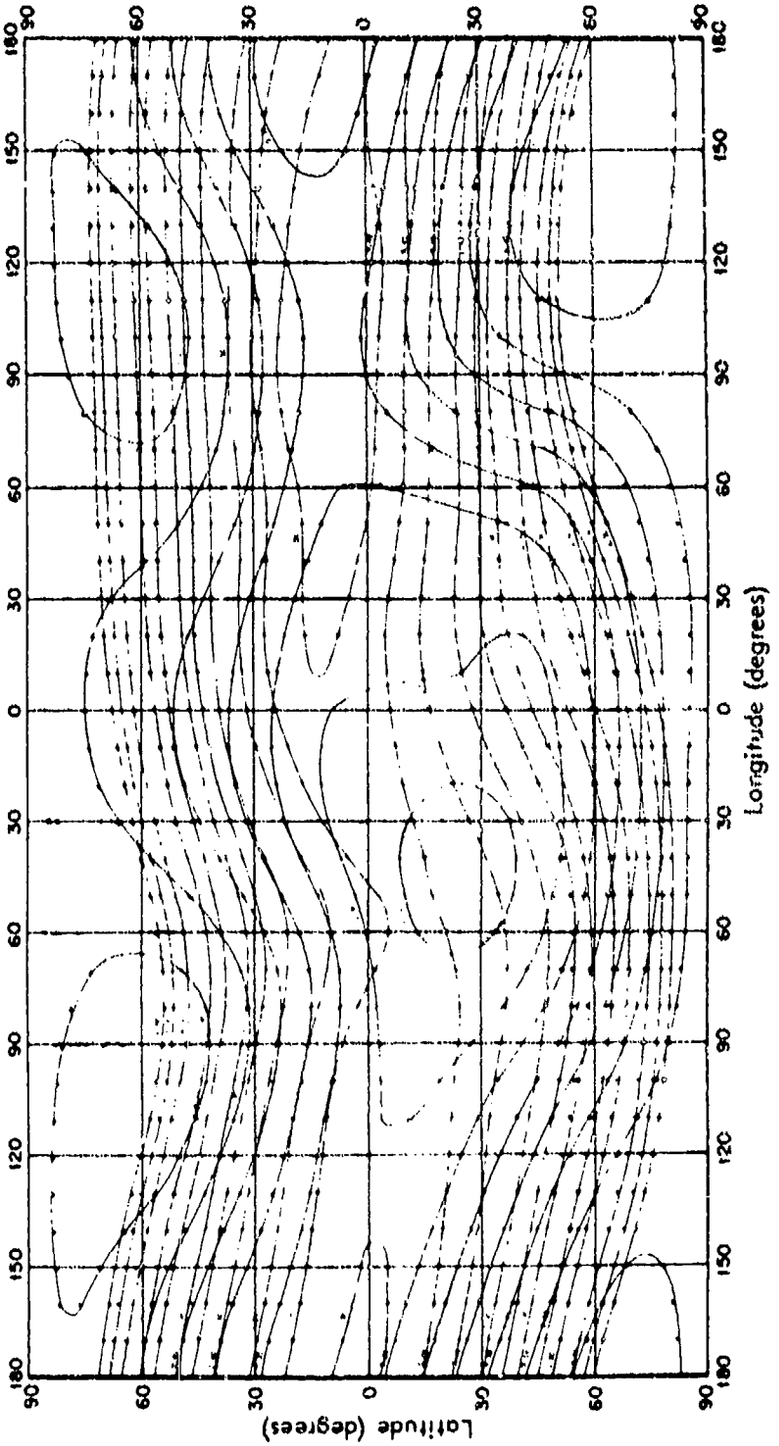

Figure 2C-1 Contours of constant-B and constant-L at 100-kilometer altitude.

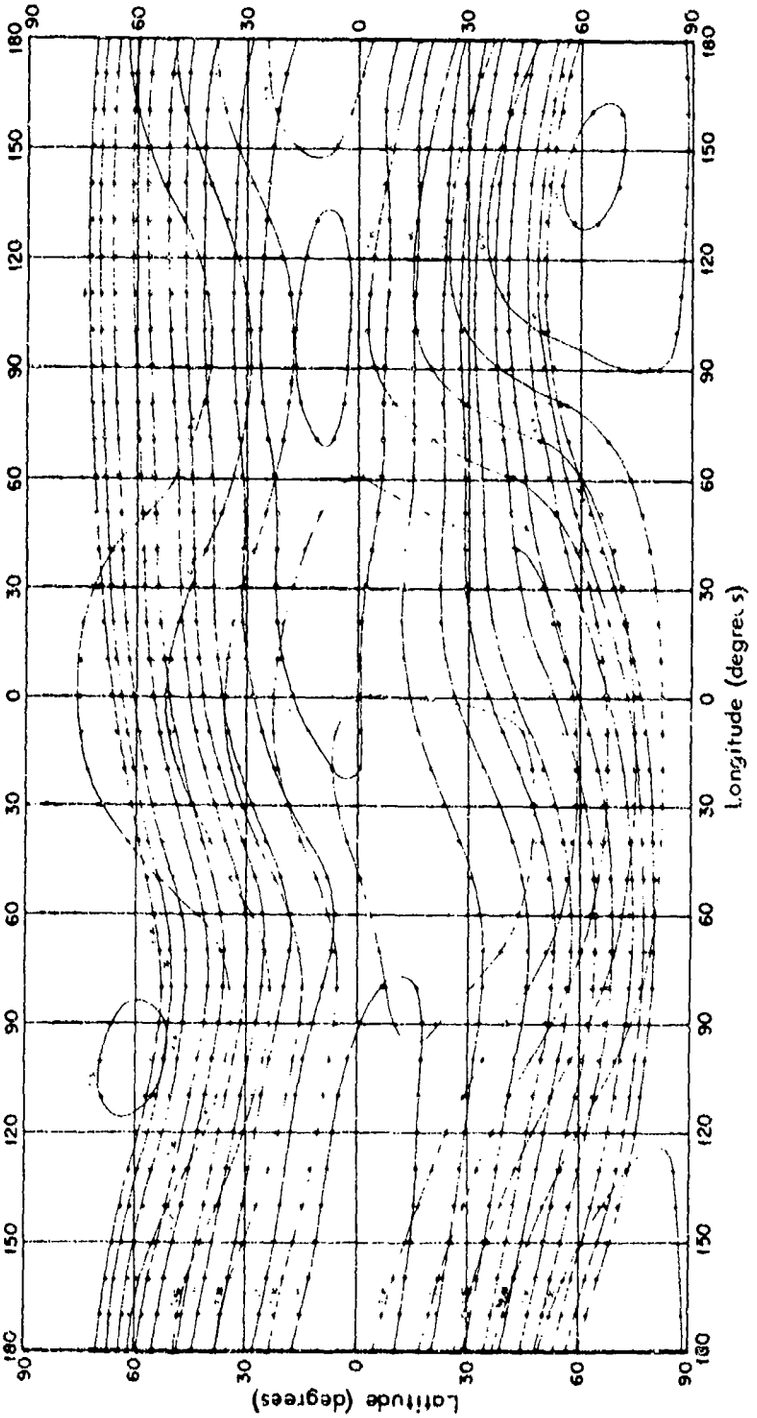

Figure 2C-2. Contours of constant-B and constant-L at 400-kilometer altitude.

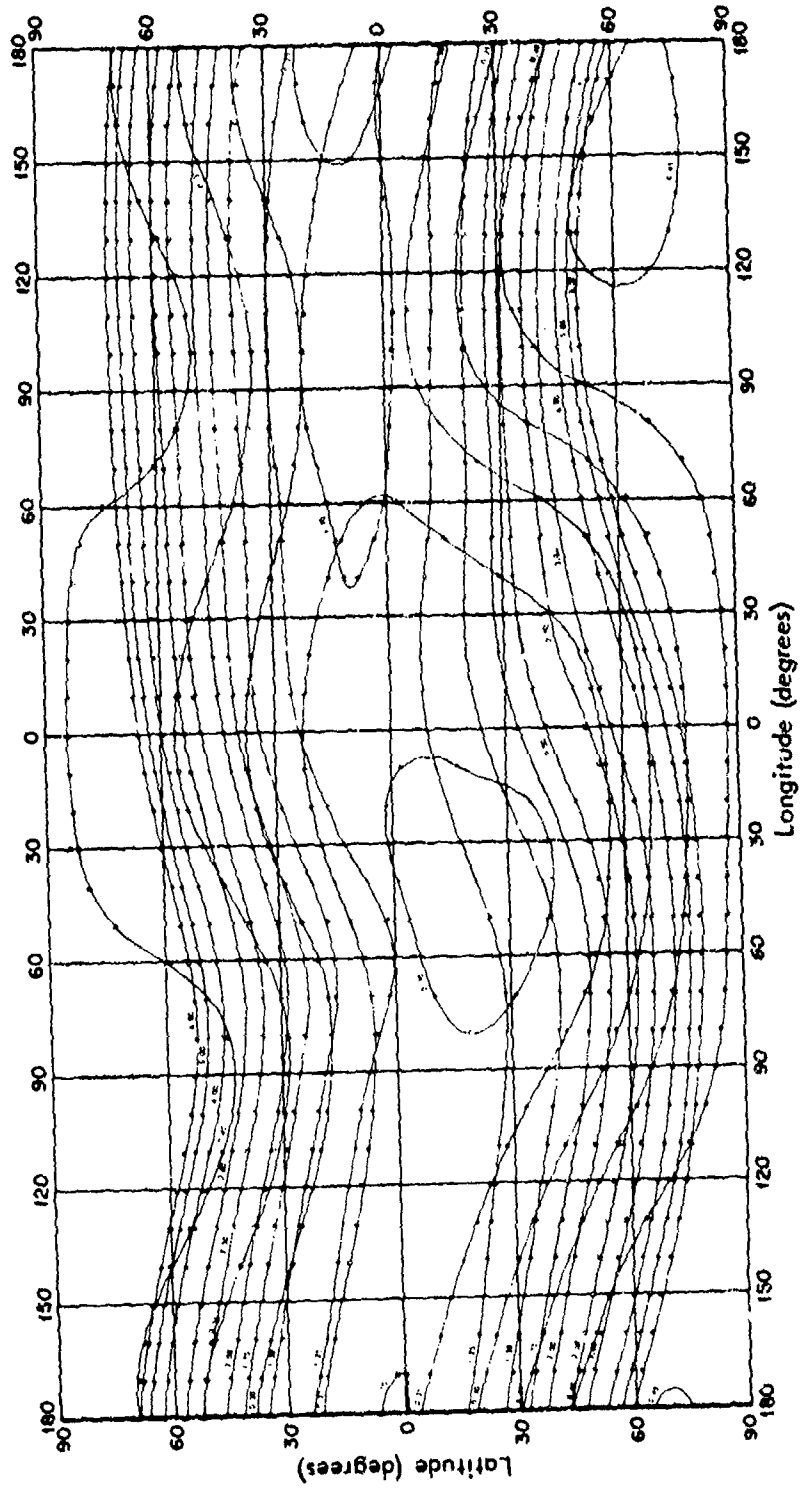

Figure 2C-3. Contours of constant-B and constant-L at 800-kilometer altitude.

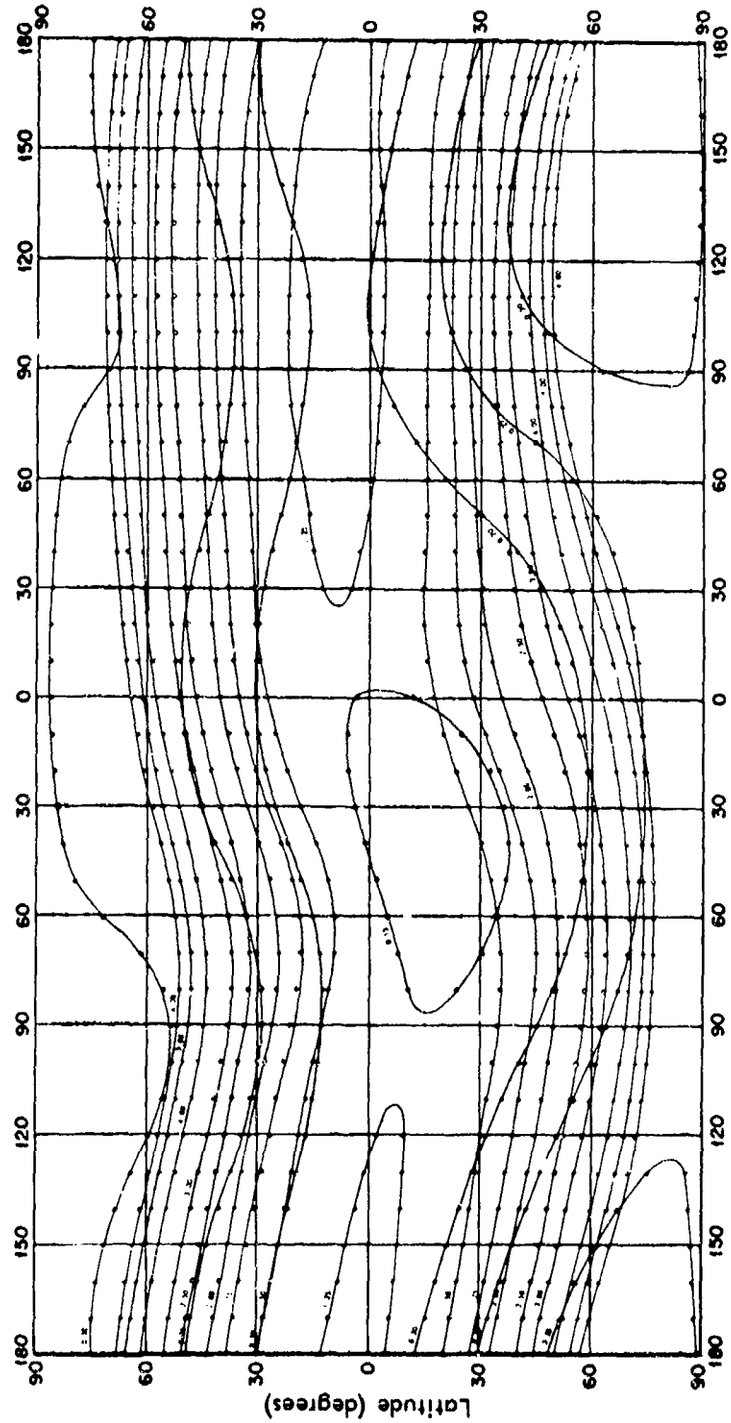

Figure 2C-4. Contours of constant-B and constant-L at 1,600-kilometer altitude.

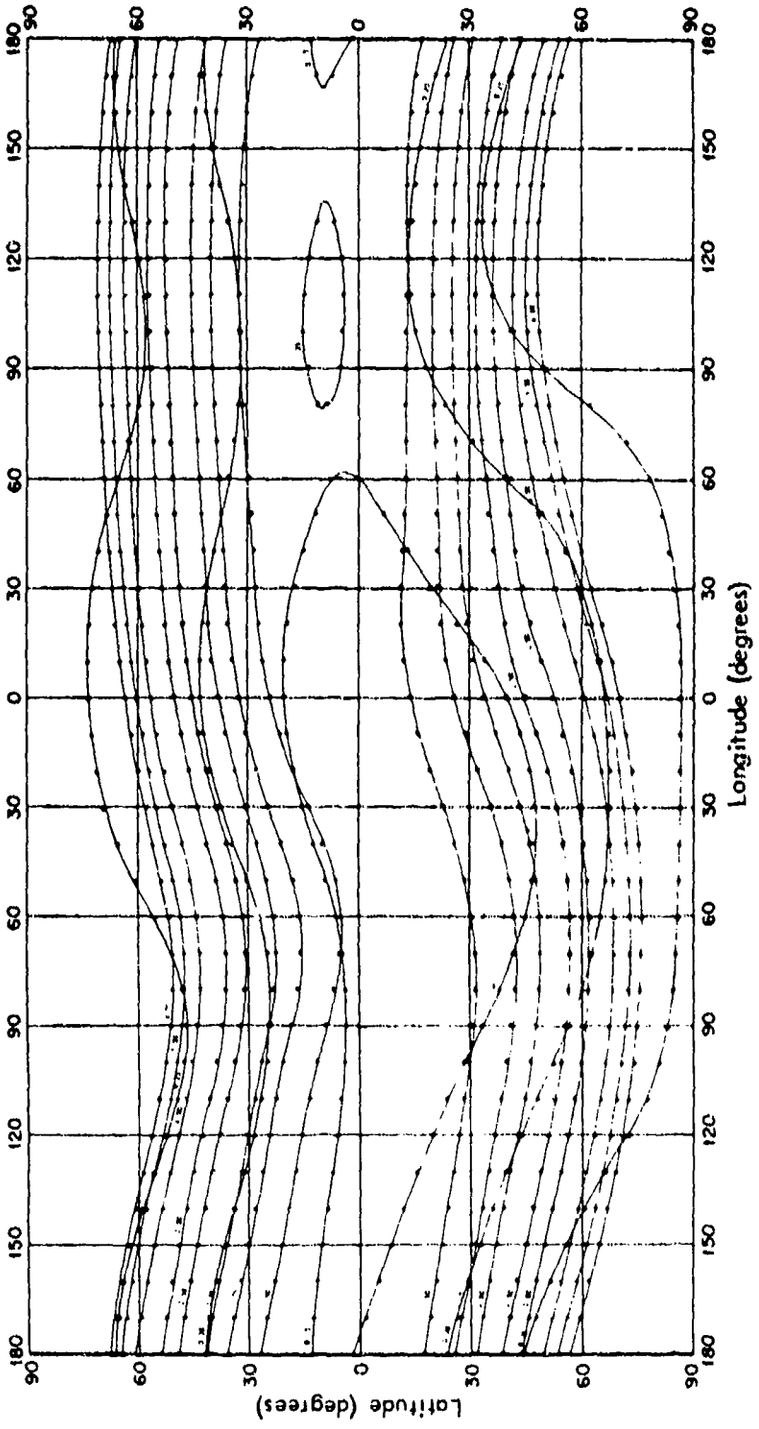

Figure 2C-5. Contours of constant-B and constant-L at 2,000-kilometer altitude.

21 January 1977

APPENDIX 2D

CONSTANT-B VERSUS ALTITUDE, LONGITUDE, AND MAGNETIC SHELL NUMBER

This appendix contains plots of altitudes of constant-B in gauss versus longitude on the magnetic shells L = 1.12, 1.20, 1.60, 2.20, and 3.50 (References 14 and 23).

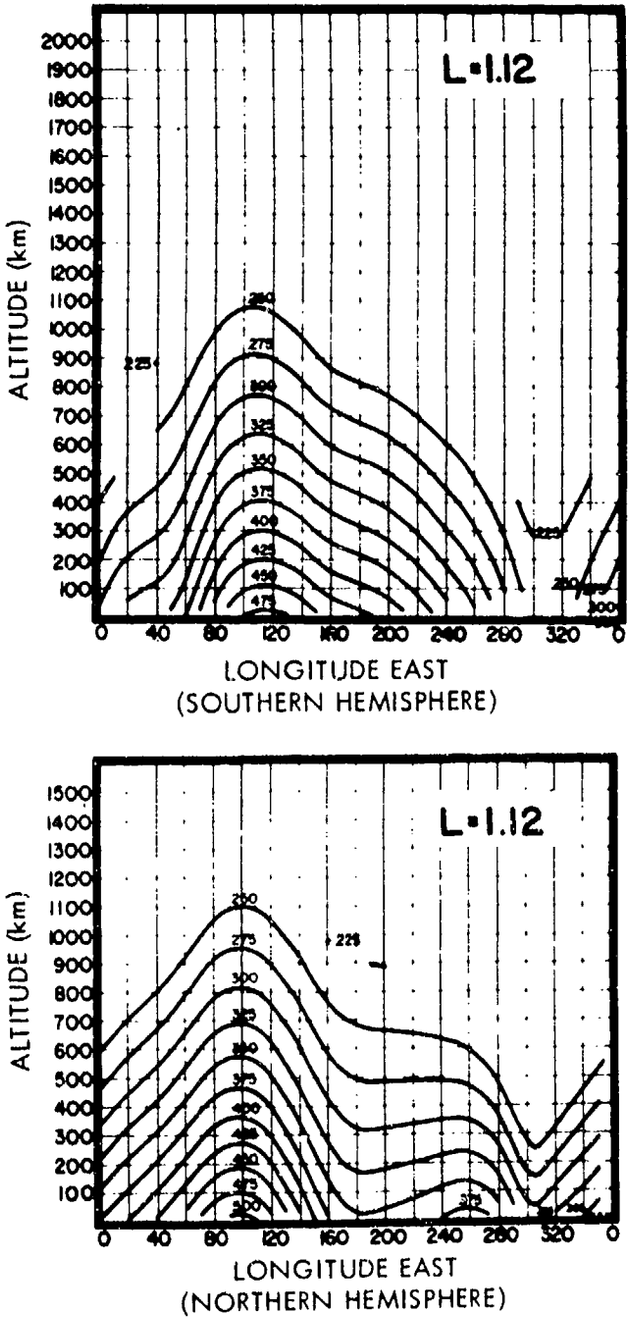

Figure 2D-1. Altitudes of constant-B for L = 1.12.

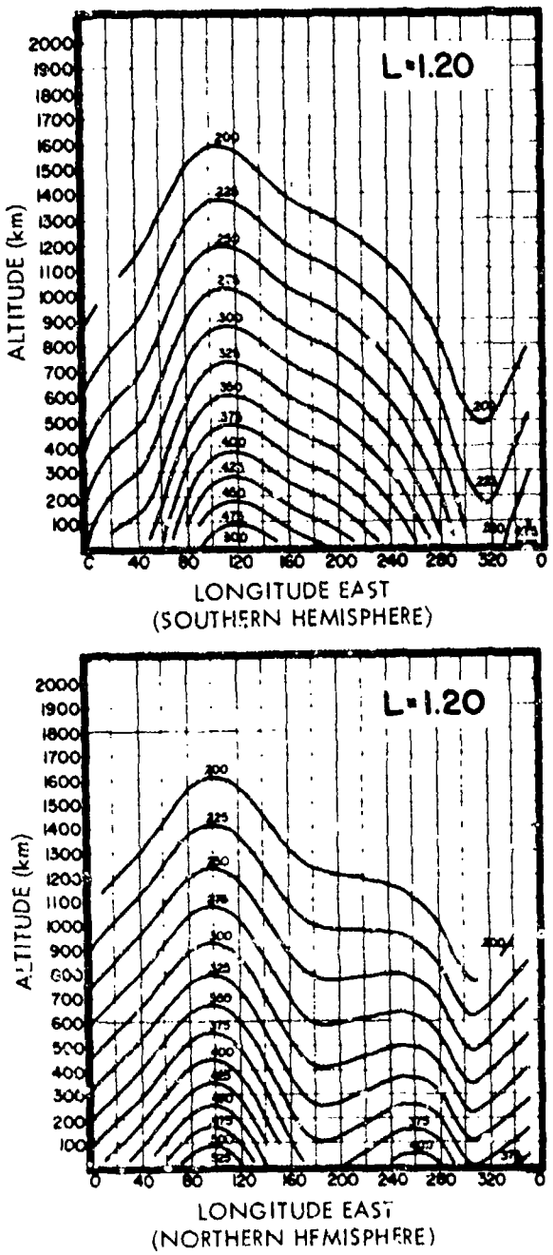

Figure 2D-2. Altitudes of constant-B for L = 1.20.

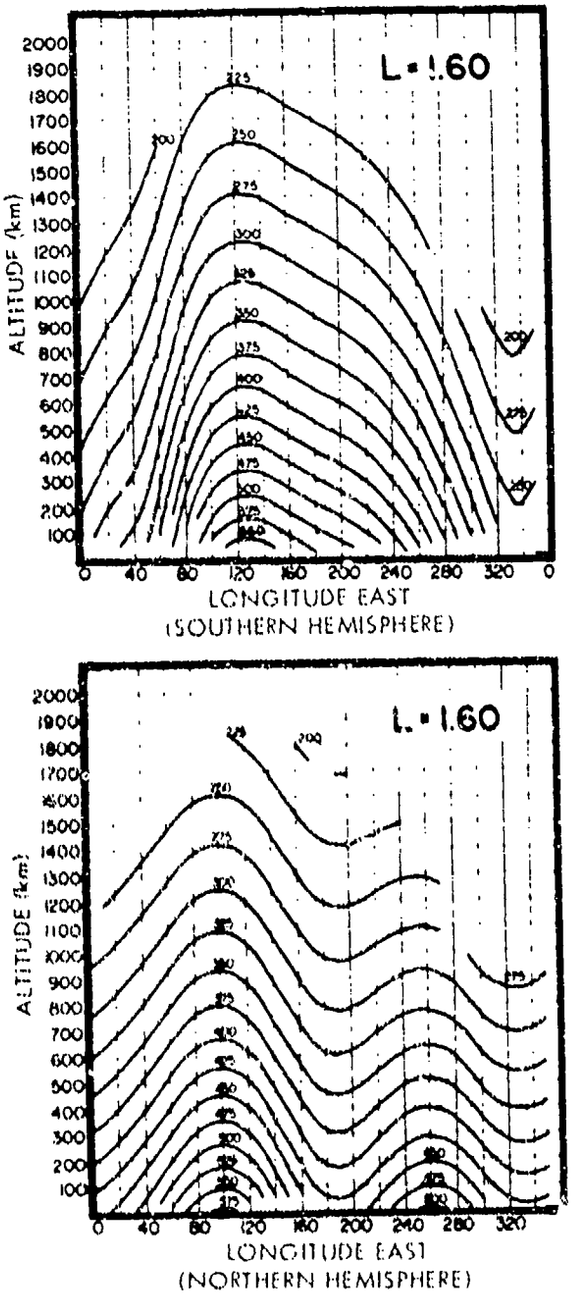

Figure 2D-3. Altitudes of constant-B for L 1.60.

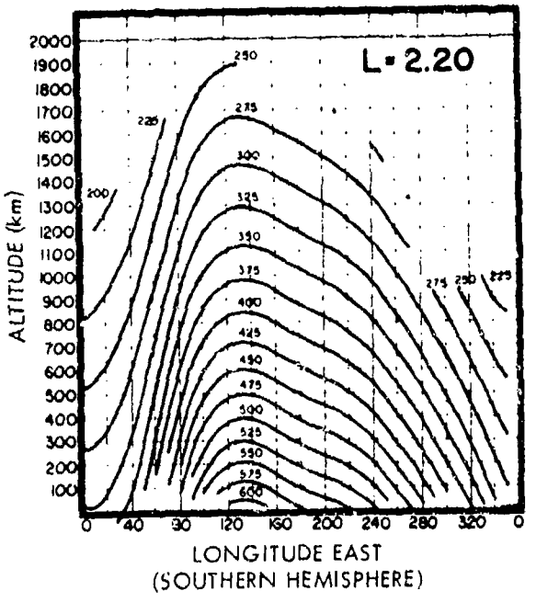

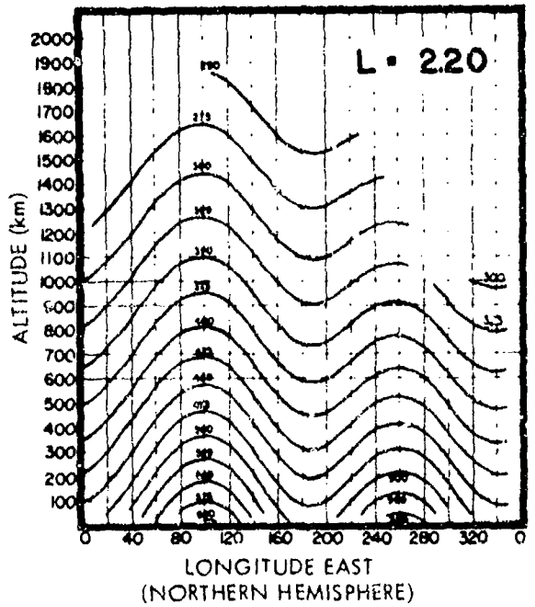

Figure 2D-4. Altitudes of constant-B for L = 2.20.

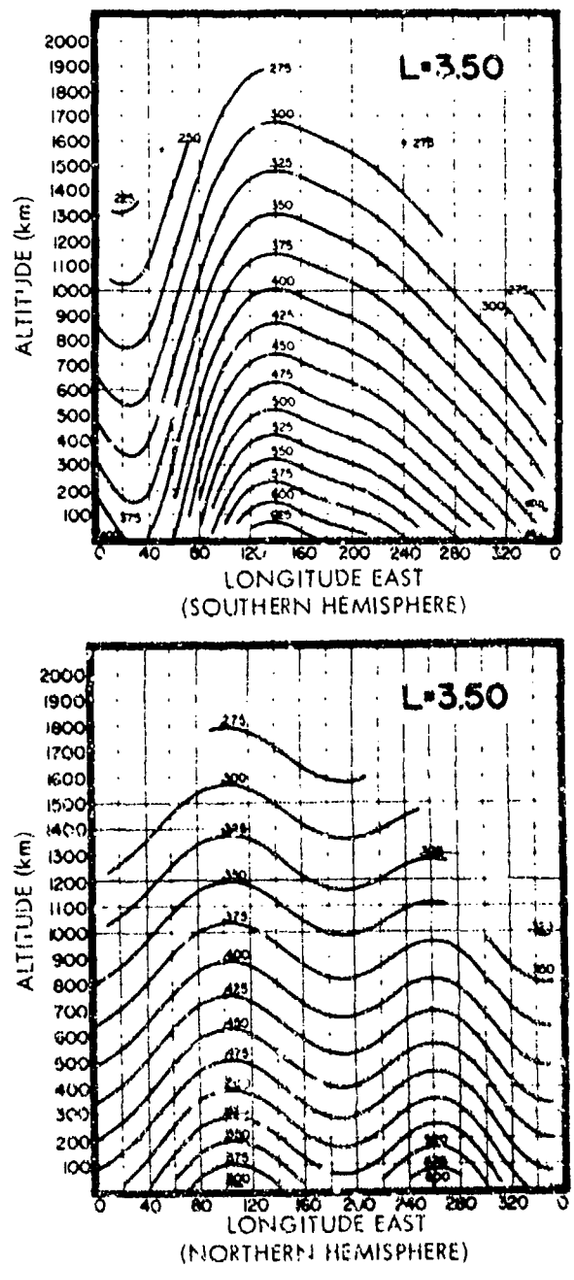

Figure 2D-5. Altitudes of constant-B for L = 3.50.

REFERENCES

1. J.C. Cain, W.E. Daniels, S.J. Hendricks, and D.C. Jensen. "An Evaluation of the Main Geomagnetic Field, 1940-1962," J. Geophys. Res., 70, 3647-3674, 1965.
2. J.C. Cain. "Structure and Secular Change of the Geomagnetic Field," Rev. Geophys. Space Phys., 13, No. 3, 203-206, 1975.
3. W.D. Parkinson and J. Cleary. "The Eccentric Geomagnetic Dipole," J. Geophys. Res., 1, 346, 1958.
4. H.T. Finch and B.R. Leaton. "The Main Magnetic Field—Epoch 1955," Geophys. Supp. RAS, 7, 314, 1957.
5. M. Abraham and R. Becker. The Classical Theory of Electricity and Magnetism, Hafner, New York, translation, 283 pp.
6. C.E. McIlwain. "Coordinates for Mapping the Distribution of Magnetically Trapped Particles," J. Geophys. Res., 66, 3681-3691, 1961.
7. J.C. Cain and S.J. Cain. "Derivation of the International Geomagnetic Reference Field," International Geomagnetic Reference Field 10/68, NASA Preprint, X-612-68-501, December 1968.
8. IAGA Commission 2, Working Group 4, Analysis of the Geomagnetic Field, "International Geomagnetic Reference Field 1965.0," J. Geophys. Res., 74, 4407-4408, 1969.
9. J.E. Evans, L.L. Newkirk, and B.M. McCormac. North Polar, South Polar, World Maps and Tables of Invariant Magnetic Coordinates for Six Altitudes: 0, 100, 300, 600, 1000, and 3000 km, DASA 2347, Lockheed Palo Alto Research Laboratory, Palo Alto, California, October 1969.
10. Handbook of Geophysics, Revised Edition, United States Air Force, The Macmillan Co., New York, 1960.
11. S. Chapman and J. Bartels. Geomagnetism, II, 609-669, Oxford University Press, London, 1940.

12. A.J. Zmuda, "A Method for Analyzing Values of the Scalar Magnetic Intensity," J. Geophys. Res., 63, 477-490, 1958.

13. D.C. Jensen and W.A. Whitaker. "A Spherical Harmonic Analysis of the Geomagnetic Field," J. Geophys. Res., 65, 2500, 1960.

14. D.C. Jensen and J.C. Cain. "An Interim Magnetic Field," J. Geophys. Res., 67, 3568-3569, 1962.

15. S.J. Hendricks and J.C. Cain. "Magnetic Field Data for Trapped Particle Evaluations," J. Geophys. Res., 71, 346-347, 1966.

16. J.C. Cain, S.J. Hendricks, R.A. Langel, and W.V. Hudson. "A Proposed Model for the International Geomagnetic Reference Field, 1965," Preprint, Goddard Spaceflight Center, Greenbelt, Maryland, 1967.

17. "World Magnetic Survey 1957-1968," IAGA Bull. No. 28, A. Zmuda ed., Paris, 1971.

18. J.C. Cain and S.J. Cain. Derivation of the International Geomagnetic Reference Field (IGRF (10/68)), NASA Tech. Note D-6237, 1971.

19. D.R. Barraclough, J.M. Harwood, B.R. Leaton, and S.R.C. Malin. "A Model of the Geomagnetic Field at Epoch 1975," Geoph. J.R. Astr. Soc., 43, 645-659, 1975.

20. N.W. Peddie and E.B. Fabiano. "A Model of the Geomagnetic Field for 1975," J. Geophys. Res., 81, 2539-2542, 1976.

21. "International Geomagnetic Reference Field 1975," IAGA, EOS Trans. Am. Geophys. U., 57, No. 3, 120-121, 1976

22. E.H. Vestine and W.L. Sibley. Geomagnetic Field Lines in Space, Rand Corp. Rept. R-368, Santa Monica, California, December 1960, 110 pp.

23. B. Venkatesan. "Isocontours of Magnetic Shell Parameters B and L," J. Geophys. Res., 70, 3771-3780, 1965.

24. G. Kluge and K.E. Lenhart. "Numerical Fits for the Geomagnetic Shell Parameter," Computer Phys. Comm., 3, 36-41, 1972.

25. R.J. Walker. "An Evaluation of Recent Quantitative Magnetospheric Magnetic Field Models," Rev. Geophys. Space Res., 14, 411-427, 1976.

26. G.D. Mead. "Deformation of the Geomagnetic Field by the Solar Wind," J. Geophys. Res., 69, 1181-1195, 1964.

27. W.P. Olson. A Scalar Potential Representation of the Tilted Magnetopause and Neutral Sheet Magnetic Fields, Paper WD-1332, McDonnell Douglas Astronautics Company, Huntington Beach, California, 1970.

28. M. Sugiura, B.G. Ledley, T.L. Skillman, and J.P. Heppner. "Magnetospheric Field Distortions Observed by OGO 3 and 5," J. Geophys. Res., 76, 7552-7565, 1971.

29. K.W. Behannon. "Geometry of the Geomagnetic Tail," J. Geophys. Res., 75, 743-753, 1970.

30. W.P. Olson. "The Shape of the Tilted Magnetopause," J. Geophys. Res., 74, 5642-5651, 1969.

31. D.J. Williams and G.D. Mead. "Night Side Magnetosphere Configuration as Obtained from Trapped Electrons at 1100 Kilometers," J. Geophys. Res., 70, 3017-3029, 1965.

32. G.D. Mead and D.H. Fairfield. "A Quantitative Magnetospheric Model Derived from Spacecraft Magnetometer Data," J. Geophys. Res., 80, 523-534, 1975.

33. A.J. Masley, W.P. Olson, and K.A. Pfitzer. "Charged Particle Access Calculations," Proc. Int. Conf. Cosmic Rays 13th, 2, 1973.

34. H. Maeda. "Variations in Geomagnetic Field," Space Science Rev., 8, 555-590, 1968.

35. S. Matsushita. "Solar Quiet and Lunar Daily Variation Fields," Physics of Geomagnetic Phenomena, I, 301-424, S. Matsushita and W.H. Campbell, eds., Academic Press, New York, 1967.

36. S. Matsushita. "Geomagnetic Disturbances and Storms," Physics of Geomagnetic Phenomena, II, 793-819, S. Matsushita and W.H. Campbell, eds., Academic Press, New York, 1967.

37. S. Chapman and J. Bartels. "The Morphology of Magnetic Disturbances," Geomagnetism, I, 272-338, Oxford University Press, London, 1940.

38. E.N. Parker. "Disturbance of the Geomagnetic Field by the Solar Wind," Physics of Geomagnetic Phenomena, II, 1153-1202, S. Matsushita and W.H. Campbell, eds., Academic Press, New York, 1967.

39. C. Rostoker and C.-G. Fälthammar. "Relationship Between Changes in the Interplanetary Magnetic Field at the Earth's Surface," J. Geophys. Res., 72, 5853-5863, 1967.

40. D.H. Fairfield and L.J. Cahill, Jr. "Transition Region Magnetic Field and Polar Magnetic Disturbances," J. Geophys. Res., 71, 155-169, 1966.

41. S. Chapman and J. Bartels. "Bays, Pulsations, and Minor Disturbances," Geomagnetism, I, 338-355, Oxford University Press, London, 1940.

42. W.H. Campbell. "Geomagnetic Pulsations," Physics of Geomagnetic Phenomena, II, 821-909, S. Matsushita and W.H. Campbell, eds., Academic Press, New York, 1967.

43. C.W. Horton and A.A.J. Hoffman. "Magnetotelluric Fields in the Frequency Range .03 to 7 Cycles per Kilosecond, 1. Power Spectra," J. Res. Natl. Bur. Stand. USA, 66D, 487-494, 1962.

44. W.H. Campbell. "Rapid Geomagnetic Field Variations Observed at Conjugate Locations," Radio Sci., 3, 726-739, 1968.

45. W.H. Campbell. "Studies of Magnetic Field Micropulsations With Periods of 5 to 30 Seconds," J. Geophys. Res., 64, 1819-1826, 1959.

46. J.B. Wilcox and E. Maple. Navord Report 4004, U.S. Naval Ordnance Lab., White Oak, Maryland, 1957.

47. L.R. Tepley and R.C. Wentworth. Structure and Attenuation of Hydromagnetic Emissions, II, 73, Lockheed Physical Sciences Laboratory, Report No. 1, AFCRL-62-32(II), Palo Alto, California, 1962.

48. M. Balser and C.A. Wagner. "Observations of Earth-Ionosphere Cavity Resonances," Nature, 188, 638-643, 1960.

49. A.D. Watt and E.L. Maxwell. "Characteristics of Atmosphere Noise from 1 to 100 kc," Proc. I.R.E., 45, 787-794, 1957.

50. A. Kimpara. "Lightning Flashes and Atmospherics," Progress in Radio Science, IV, 5-12, F. Horner, ed., Elsevier Publishing Co., New York, 1965.

51. A.L. Hales. "A Possible Mode of Propagation of the 'Slow' or 'Tail' Component in Atmospherics," Proc. Roy. Soc. London, A, 193, 60-71, 1948.

52. T. Madden and W. Thompson. "Low-Frequency Electromagnetic Oscillations of the Earth-Ionosphere Cavity," Rev. Geophys., 3, 211-254, 1965.

53. D.A. Gurnett, S.D. Shawhan, N.M. Brice, and R.L. Smith. "Ion Cyclotron Whistlers," J. Geophys. Res., 70, 1665-1688, 1965.

54. A. Egeland, G. Gustaffson, S. Olsen, J. Aarons, and W. Barron. "Auroral Zone Emissions Centered at 700 Cycles per Second," J. Geophys. Res., 70, 1079-1082, 1965.

55. R.A. Helliwell. Whistlers and Related Ionospheric Phenomena, Stanford University Press, Stanford, California, 1965, 349 pp.

56. J.V. Lincoln, "Geomagnetic Indices," Physics of Geomagnetic Phenomena, I, 67-100, S. Matsushita and W.H. Campbell, eds., Academic Press, New York, 1967.

57. W.F. Dudziak, D.D. Kleinecke, and T.J. Kostigen. Graphic Displays of Geomagnetic Geometry, RM63TMP-2, DASA 1372, General Electric Co., Santa Barbara, California, 1963, 60 pp.

SECTION 15
INDEX